


# Strategies to Regulate the Degradation and Clearance of Mesoporous Silica Nanoparticles: A Review

Yuelin Zhang, Xue Lin, Xinxin Chen, Weixiang Fang, Kailing Yu, Wenting Gu, Yinghui Wei, Hangsheng Zheng, Jigang Piao , Fanzhu Li

School of Pharmaceutical Sciences, Zhejiang Chinese Medical University, Hangzhou, 310053, People's Republic of China

Correspondence: Fanzhu Li; Ji-Gang Piao, Email lifanzhu@zcmu.edu.cn; jgpiao@zcmu.edu.cn

**Abstract:** Mesoporous silica nanoparticles (MSNs) have attracted extensive attention as drug delivery systems because of their unique meso-structural features (high specific surface area, large pore volume, and tunable pore structure), easily modified surface, high drug-loading capacity, and sustained-release profiles. However, the enduring and non-specific enrichment of MSNs in healthy tissues may lead to toxicity due to their slow degradability and hinder their clinical application. The emergence of degradable MSNs provided a solution to this problem. The understanding of strategies to regulate degradation and clearance of these MSNs for promoting clinical trials and expanding their biological applications is essential. Here, a diverse variety of degradable MSNs regarding considerations of physiochemical properties and doping strategies of degradation, the biodistribution of MSNs in vivo, internal clearance mechanism, and adjusting physical parameters of clearance are highlighted. Finally, an overview of these degradable and clearable MSNs strategies for biosafety is provided along with an outlook of the encountered challenges.

**Keywords:** mesoporous silica nanoparticles, degradation, clearance, biodistribution, strategies

## Introduction

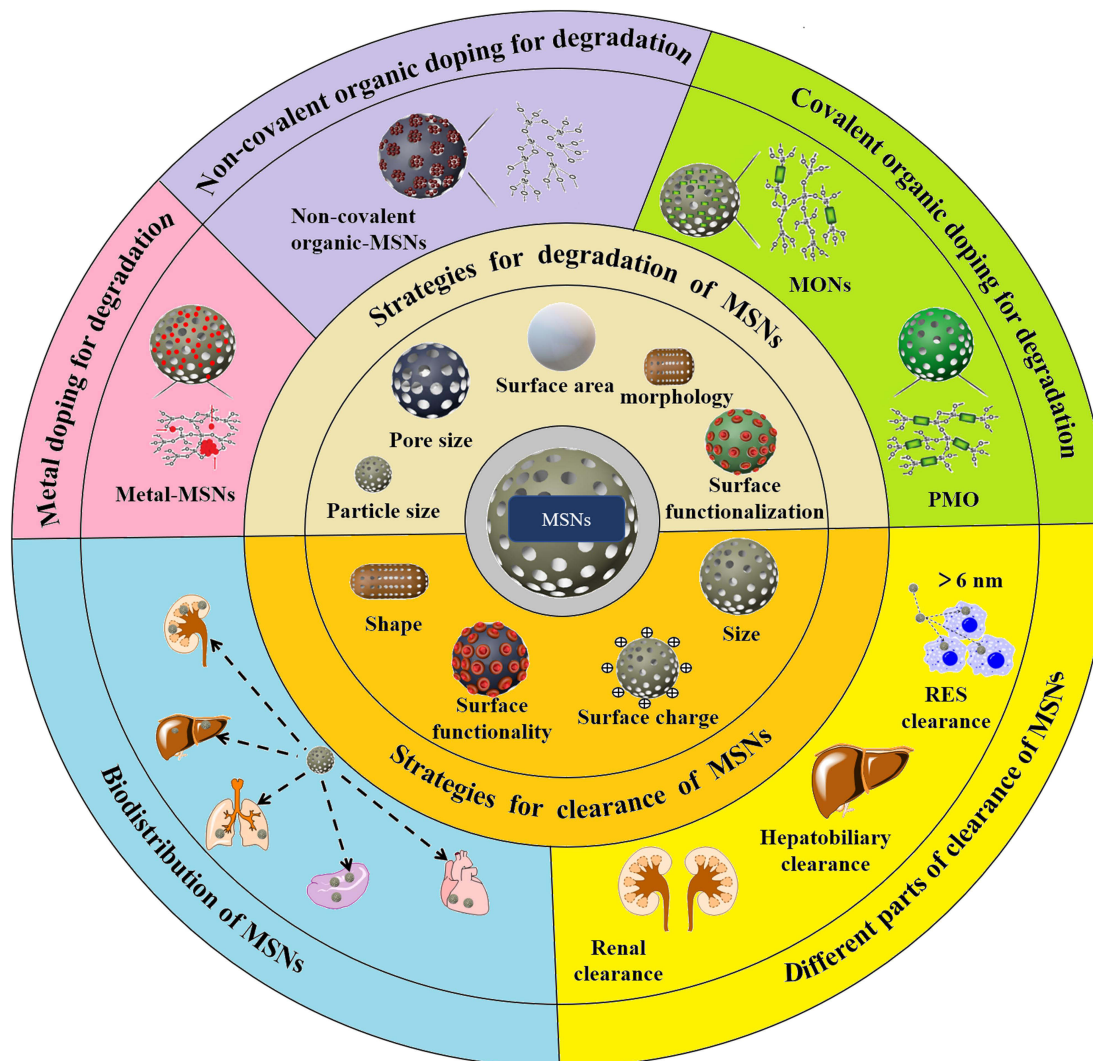
MSNs have emerged as a prominent nanomaterial with growing interest, primarily due to their excellent biocompatibility, tunable pore size, large surface area, and abundant surface ease of functionalization. Their unique properties have positioned them as a significant focus of research and development as nanocarriers in drug delivery.<sup>1–12</sup> However, many studies have reported that slow biodegradability of MSNs could lead to severe particle bioaccumulation, potentially resulting in biosafety problems.<sup>13–16</sup> Generally, the degradation process of MSNs took several days, and the excretion of MSNs took several weeks from the body.<sup>17,18</sup> Therefore, improving the degradation of MSNs for facilitating in vivo studies and clinical trials has become an urgent necessity. Moreover, the requirements of the US Food and Drug Administration (FDA), agents injected into the human body, especially diagnostic ones, must be completely cleared within a reasonable period after achieving the purpose.<sup>19</sup> Systematic evaluations of the degradation behavior and clearance of MSNs in vivo are critical for the achievement of clinical translation and expansion of disease therapeutic applications.<sup>20,21</sup>

In view of the extensive research on the degradation and clearance of MSNs,<sup>22–29</sup> This paper will systematically overview the strategies to regulate degradation and clearance of MSNs, with highlights on degradation behavior about organic doping and metal doping, and clearance mechanisms and adjusting physical parameters for clearance. We believe that this review can provide readers with more information on the optimal method to achieve degradation of MSNs and better understand the mechanism of clearance.

## The Degradation of MSNs

The degradation of MSNs is a hydrolytic dissolution process, which occurs by the nucleophilic interaction between hydroxyl groups in aqueous media and non-bridged oxygen on MSNs surface, leading to the leach of dissoluble silicic acid.<sup>5</sup> Croissant et al summarized the mechanism of MSNs degradation in an aqueous medium which is divided into three steps: (1) hydration, water molecules are adsorbed to the siloxane skeleton, (2) hydrolysis, siloxane is hydrolyzed to

## Graphical Abstract



silanol, and (3) ion-exchange, hydroxyl anion nucleophilic attacks, eventually forming silicic acid.<sup>28</sup> In recent years, in addition to regulating the degradation of MSNs by adjusting the physical and chemical properties, studies have also focused on improving the biodegradability of MSNs by reconstructing the silica skeleton, such as constructing organic-inorganic hybrid structures (Si-O-R), or introducing metal ions or metal oxides for doping. Among them, the organic group R has a certain protective effect on silica, making the Si-O-Si skeleton more stable, and using reducible and degradable organics for doping can effectively improve the degradability of MSNs.<sup>30–35</sup>

## Degradation of MSNs by Regulating Physicochemical Properties

The degradation rate of MSNs depends on two categories of parameters: (i) the particle characteristics (surface area, particle size, pore size, morphology, condensation degree, hydrophilicity/hydrophobicity, surface functional groups, etc.) and (ii) the degradation medium characteristics (protein presence or absence, concentration, etc.).<sup>28</sup> Kuroda et al provided findings on the degradation rates of MSNs having equivalent surface areas (960–980 m<sup>2</sup>/g). However, these MSNs with equal surface areas were no significant differences observed in the degradation rates of MSNs with varying particle sizes (20 nm, 30 nm, 40 nm, 80 nm) (Figure 1A–B). This indicated that the degradability of MSNs was unrelated to their size

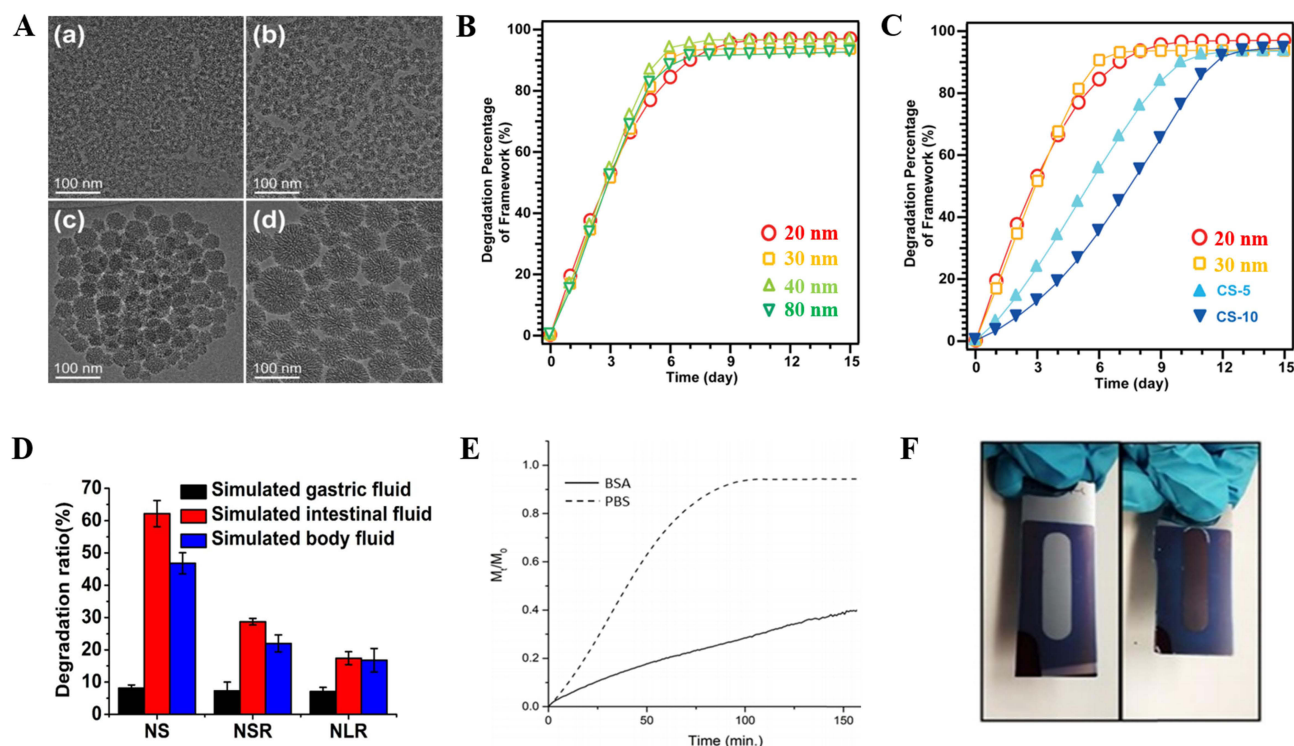


**Figure 1** Degradation of MSNs by regulating physicochemical properties.

**Notes:** (A) TEM images of 20 nm (a), 30 nm (b), 40 nm (c), and 80 nm (d) MSNs. (B) Degradation percentages of different particle sizes. (C) Degradation percentages of different mesoporous structures (20 nm MSNs, 30 nm MSNs, CS-5, and CS-10). Reprinted from Yamada H, Urata C, Aoyama Y et al. Preparation of colloidal mesoporous silica nanoparticles with different diameters and their unique degradation behavior in static aqueous systems. *Chem. Mater.* 2012;24(8):1462–1471. Copyright 2012 with permission from American Chemical Society.<sup>24</sup> (D) Quantitative data of degradation rate of NS, NSR, and NLR in simulated gastric, intestinal, and body fluid. Reprinted from Li LL, Liu TL, Fu CH et al. Biodistribution, excretion, and toxicity of mesoporous silica nanoparticles after oral administration depends on their shape. *Nanomedicine.* 2015;11(8):1915–1924. Copyright 2015 with permission from Elsevier.<sup>36</sup> (E) Dissolution curves of MSNs at 37 °C in PBS and in BSA solution. (F) Picture of MSNs films after 3 h of dissolution in PBS (left) and BSA solution (right). Reprinted from Bindini E, Chehadi Z, Faustini M et al. Following in situ the degradation of mesoporous silica in biorelevant conditions: at last, a good comprehension of the structure influence. *ACS. Appl. Mater. Interfaces.* 2020;12(12):13,598–13,612. Copyright 2020 with permission from American Chemical Society.<sup>37</sup>

but was associated with surface area. Furthermore, the degradability of the colloidal silica nanoparticles 5 nm (CS-5) and 10 nm (CS-10) silica (Figure 1C) was much lower than that of the above-mentioned MSNs. That was because MSNs had a larger contact area compared to colloidal silica nanoparticles (non-mesoporous structures).<sup>24</sup> Similarly, the degradation rates of spherical, ellipsoidal, and rod-shaped MSNs gradually slowed down with the decrease of the specific surface area. Liu et al found that the degradation process of MSNs with spherical and rod-like morphologies slowed down with the increase in aspect ratio.<sup>36</sup> In 7 d, spherical-shaped MSNs (NS) degraded by 45–65%, and short-rod-shaped (NSR) and long-rod-shaped (NLR) nanorods (Figure 1D) degraded by 25–30% and 15% in simulated intestinal fluid (SIF) or body fluid (SBF), respectively. To more closely simulate the biological environment, degradation experiments were conducted in a solution containing protein at concentrations equivalent to those present in the blood. In the presence of proteins, the dissolution rate of MSNs was relatively slow (Figure 1E), which may be attributed to the diffusion barrier effect caused by protein adsorption on the surface. Moreover, as observed in the images, after 3 h in PBS solution, silicon was no longer present, indicating the degradation of the silicon substrate. In contrast, after 3 h in BSA solution, a thick layer of silica still persisted (Figure 1F).<sup>37</sup> In addition, wettability related to hydrophilicity has been proven to be crucial for controlling the biological activity of solid particles by affecting their affinity with liquid interfaces and substances in the body. A piece of data indicated that the wettability and degradation of MSNs are similar, that is, the higher the wettability, the smaller the contact angle, and the larger the contact area, which leads to rapid material transfer and a greater likelihood of degradation.<sup>38</sup>

Considering the diverse physicochemical properties and degradation kinetics of each MSNs system, researchers can choose the optimal nanoplatform for specific applications. If an extended circulation time is required, whether MSNs are used for imaging or as delivery platforms for prolonged applications, their surface area should be kept as low as possible

without compromising their function. Conversely, if rapid degradation is needed, a high surface area is preferable. In addition, when designing MSNs as drug delivery platforms, a major concern is preventing their aggregation, and surface functionalization can also stabilize their degradation.<sup>39,40</sup> But at the same time, it will also bring about the result of slow degradation. For example, the main reason for the slow degradation could be ascribed to the presence of the PEG shell on the surface of MSNs. PEG with its hydrophilicity could resist the adhesion and prevent the adsorption of proteins, thereby reducing undesired interactions between the physiological environment and MSNs. Notably, the degradation rate of MSNs that were functionalized with longer and denser PEG chains was found to be slower as compared to those MSNs functionalized with shorter PEG chains.<sup>29</sup> Furthermore, the degradation behavior closely resembling the in-vivo environment will be a key research direction in the study of MSNs degradation.<sup>41</sup>

## Degradation of MSNs by Organic Doping

The degradation rate of MSNs can also be regulated and controlled by the doping of organic compounds. To achieve this, two principal strategies have been employed: one is to dope organics non-covalent molecules into MSNs, thereby forming a weakly condensed environment in the silica matrix that can accelerate hydrolytic degradation. The other is to covalently dope organic bridged alkoxysilanes into MSNs or obtain by the use of 100% of one or more bis- or multi-bridged organosilane precursors, when no additional silane source is present, and the degradation is triggered by redox reaction or enzyme reaction.

### Non-Covalent Organic Doping

Non-covalent organic doping is a physical doping method. The incorporation of organic molecules into MSNs matrix or wrapping on the surface is one of the most commonly used methods to promote biodegradation.<sup>28</sup> It reduces the densification matrix of MSNs, or destroys the skeleton structure of MSNs, and accelerates the hydrolysis of MSNs. Organic molecules such as methylene blue,<sup>42</sup> doxorubicin,<sup>43</sup> and starch,<sup>44</sup> have been used as accelerators for degrading MSNs. While these additives have to some extent promoted the biodegradation of MSNs, many issues, including unpredictable toxicity and complex preparation processes, still hinder their further clinical application.

Mannose (Man) is a common water-soluble monosaccharide, which is widely found in plants and microorganisms. To date, there have been no reports of toxicity to humans.<sup>45</sup> Hydroxyls rich in monosaccharides can easily form hydrogen bonds with the hydroxyls of MSNs, making MSNs doped with mannitol easy to prepare. In addition, the abundant source of mannitol from natural products is advantageous for reducing production costs and promoting clinical translation.<sup>46</sup> Another study started from simplifying the process providing a simple technique to manufacture a multifunctional drug carrier with degradability. MSNs were post-functionalized with a positively charged random copolymer through simple electrostatic interactions. After electrostatic blocking, the polymer-wrapped MSNs were crosslinked with dithiothreitol. The loaded drug was released through the degradation of the polymer shell in the intracellular microenvironment, inducing cell death and further degradation of the MSNs (Figure 2A).<sup>47</sup>

### Mesoporous Organosilica Nanoparticles

The design of MSNs containing organic bridged alkoxysilane in the framework of silica, which could be degraded under specific control conditions, may become a research hotspot for future clinical transformation. Mesoporous organosilica nanoparticles (MONs) were designed by bridging two or more organ alkoxysilane, a rapidly rising field in the research of mesoporous silica.<sup>50–55</sup> Organic bridged alkoxysilanes combined covalent bonds included disulfide bond (-S-S-), sulfide bond (-S-S-S-S-), diselenide bond (-Se-Se-), amide bond (-CO-NH-), which were connected to the silica skeleton to achieve degradation by redox reaction or enzymatic reaction. The degradation trend at different times of MONs by redox reaction or enzymatic reaction was listed in Table 1.

The structure of the disulfide (-S-S-) was mainly triggered by glutathione (GSH) to cause the silica skeleton structure fracture to achieve degradation.<sup>48,61</sup> Yang et al reported the first cancer cell-specific degradable dendritic MONs.<sup>48</sup> The unique pore structure dependent GSH-responsive degradation behavior showed that the degradation rates of two nanoparticles with different pore sizes were similar in normal cells, while macroporous MONs showed faster degradation rates than small pore MONs in cancer cells with relatively higher intracellular GSH levels (Figure 2B). Similarly, the addition of a thioether bond



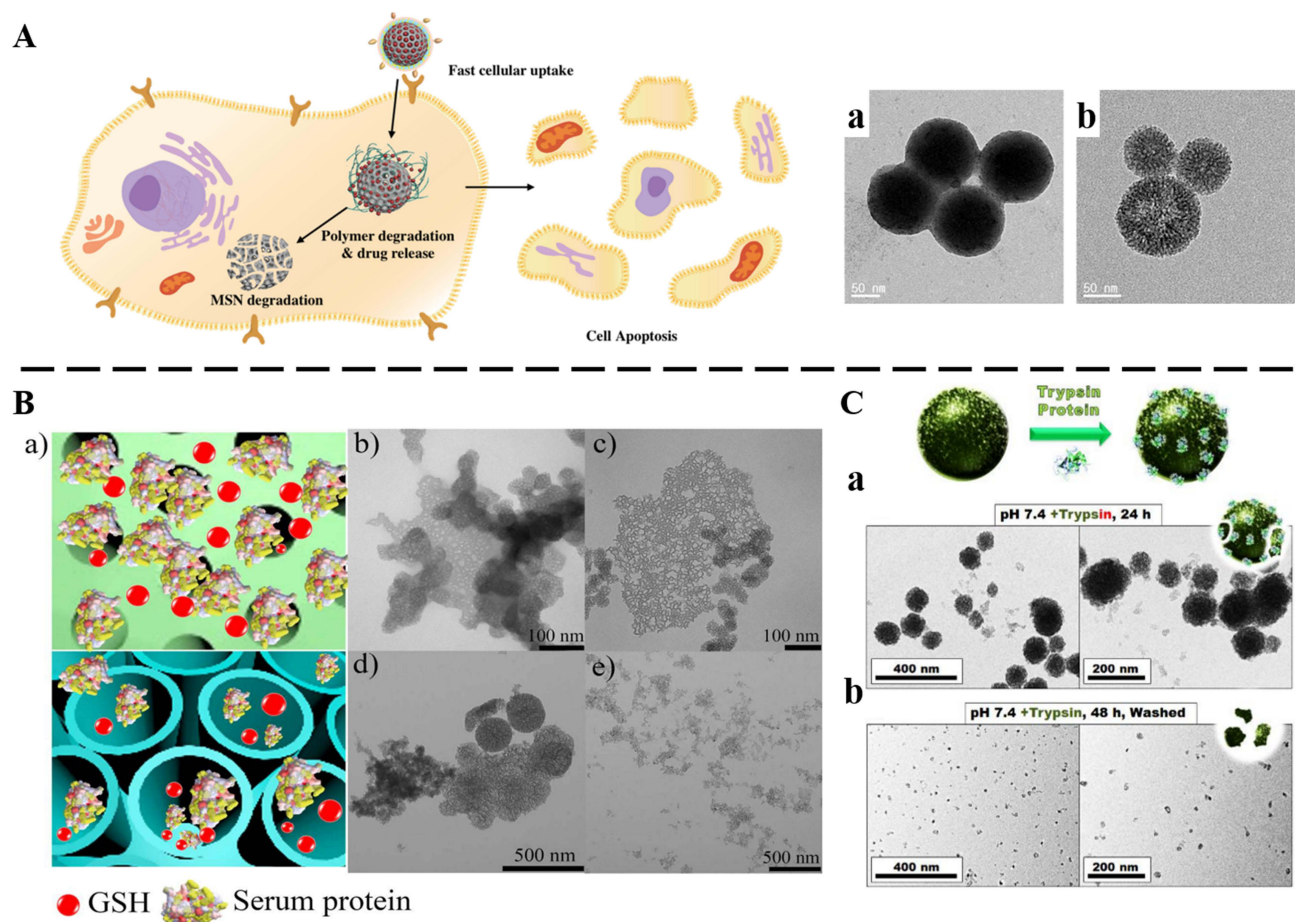


**Figure 2** Covalently organic doped MSNs for degradation.

**Notes:** (A) Schematic illustration of the fast cellular uptake analysis by the polymer MSNs and their redox responsive drug release. TEM images of the polymer MSNs (a) before and (b) after 30 d in PBS with GSH. Scale bar represents 50 nm. Reprinted from Palanikumar L, Kim J, Oh JY et al. Hyaluronic acid-modified polymeric gatekeepers on biodegradable mesoporous silica nanoparticles for targeted cancer therapy. *ACS Biomater Sci Eng.* 2018;4(5):1716–1722. Copyright 2018 with permission from American Chemical Society.<sup>47</sup> (B) Schematic illustration of the role of GSH in the pore structure-dependent degradability (a). TEM images of small pore MONs (b, c) and macroporous MONs (d, e) were incubated in 10 mM GSH solution for 24 h (b, d) and 48 h (c, e). Reprinted from Yang Y, Wan J, Niu Y et al. Structure-dependent and glutathione-responsive biodegradable dendritic mesoporous organosilica nanoparticles for safe protein delivery. *Chem. Mater.* 2016;28(24):9008–9016. Copyright 2016 with permission from American Chemical Society.<sup>48</sup> (C) Representation of the surface coating of proteins on MONs, involved during the NPs degradation. TEM micrographs of degraded MONs after 24 (a) and 48 h (b) in PBS with trypsin. Reprinted from Croissant JG, Fatieiev Y, Julfakyan K et al. Biodegradable oxamide-phenylene-based mesoporous organosilica nanoparticles with unprecedented drug payloads for delivery in cells. *Chemistry.* 2016;22(42):14,806–14,811. Copyright 2016 with permission from Wiley.<sup>49</sup>

(-S-S-S-) also could render nanoparticles easily degraded by biological redox stimulation.<sup>56,57</sup> Wang et al synthesized colloidal MSNs, and hybrid colloidal MSNs incorporated thioether bonds.<sup>56</sup> The degradation percentages of colloidal MSNs and hybrid colloidal MSNs after 7 d were 78% and 60% in pH 7.4 SBF, respectively. However, in a high-concentration reducing medium containing dithiothreitol (DTT), the degradation rate of hybrid colloidal MSNs with 92% was faster than that of colloidal MSNs with 82% after 7 d. The above results showed that in a high-concentration reducing environment, the hybrid colloidal MSNs carrier exhibited a faster degradation rate due to the rupture of the sulfide bond. The diselenide bond (-Se-Se-) was also bonded into the silica framework and was cleaved by the GSH environment of TME to achieve the purpose of degradation. Compared with sulfur, selenium has a larger atomic radius and weaker electronegativity, resulting in lower bond energies. Selenium could be oxidized to form selenite or reduced to form selenol and diselenide under different redox conditions, and the diselenide bond was more easily broken.<sup>62</sup> To prepare mesoporous organic silica, Shao et al introduced the diselenide bond (-Se-Se-) into the framework of MONs.<sup>58</sup> The degradation behavior of organic silica was studied under the medium of simulating oxidative conditions ( $\text{H}_2\text{O}_2$ ,  $100 \times 10^{-6}$  M) or reduced conditions (GSH,  $5 \times 10^{-3}$  M). TEM image showed that after 1 d of incubation, the selenium-based organic silica was rapidly degraded. After 3 d, the structure of organic silica was broken down into small fragments. In contrast, the sulfur-based organic silica showed that the

**Table 1** Degradation Trend at Different Time of MONs by Redox Reaction or Enzymatic Reaction

Redox /Enzymatic Reaction	Chemical Bonds/Metal	Degradation Trends at Different Time	Ref.
Redox reaction (GSH)	-S-S-	The material completely decomposed into small fragments in a serum containing 10 mM GSH after 48 h.	[48]
Redox reaction (DTT)	-S-S-S-S-	A degradation rate of 92% was observed in the presence of 5 mM DTT after 7 d.	[56]
Redox reaction (GSH)	-S-S-S-S-	The dendritic shell was completely degraded after 2 d, and the entire pore structure was almost destroyed after 5 d.	[57]
Redox reaction (GSH) ROS condition (H <sub>2</sub> O <sub>2</sub> )	-Se-Se-	The material rapidly degraded after 1 d of incubation, broken down into small fragments in 100×10 <sup>-6</sup> M H <sub>2</sub> O <sub>2</sub> and 5×10 <sup>-3</sup> M GSH after 3 d.	[58]
Enzymatic reaction	-CO-NH-	The material cracked at 24 h, and degraded to 20 nm in pH 7.4 PBS containing trypsin at 48 h.	[49]
Redox reaction (GSH)	-S-S- +Fe <sup>2+</sup>	The surface structure dissociated in the presence of 10 mM GSH within 12 h, and the frame gradually collapsed after 24 and 48 h.	[59]
Redox reaction (GSH)	-S-S-S-S-+Cu <sup>2+</sup>	Most of the nanosheets were destroyed in the presence of 10 mM GSH after 14 d.	[60]

structure was damaged under reduced conditions, but not in oxidative conditions. Therefore, nanoparticles constructed with the diselenide bond had the dual response effects of redox reactions. In addition, an amide bond (-CO-NH-) in response to the enzymatic reaction caused rapid degradation of MONs. Jonas et al synthesized oxamide-phenylene-based MONs without a silicon source.<sup>49</sup> In the presence of trypsin model proteins, the shell of MONs cracked at 24 h, and degraded to around 20 nm at 48 h (Figure 2C). The selective protein-mediated degradation was further verified by controls using denatured trypsin (heated at 95 °C for 7 minutes), which did not cause significant size changes for MONs. This result strongly illustrated the enzymatic mechanism of degradation.

As treatment strategies have evolved, the combination of multiple types of treatment has become common, including chemotherapy, radiotherapy, chemodynamic therapy, photothermal dynamic therapy, and photothermal therapy, which have achieved better results than a single treatment.<sup>63–65</sup> Relative to MONs, organic silica with GSH response was doped with metal ions, which could not only realize multiple therapeutic treatment, but also achieved the purpose of faster degradation. Liu et al designed -S-S- bond-rich dendritic MONs as GSH-depleting agents with iron dots and a catalase inhibitor co-loaded inside to achieve degradation and enduring chemodynamic therapy.<sup>59</sup> The surface structure of dendritic MONs dissociated after 12 h of incubation with 10 mM GSH, and the frame gradually collapsed after 24 and 48 h of incubation. Similarly, another literature also achieved through the combination of disulfide bond (-S-S-) for degradation. Cheng et al prepared a near-infrared laser-assisted and disulfide bond (-S-S-) bridged organosilica coated gold nanorods containing photosensitizer and anticancer drug doxorubicin for the treatment of breast cancer.<sup>66</sup> The degradability of nanohybrids was observed by Bio-TEM, and 4T1 cells and nanohybrids were incubated for 3, 12, and 24 h. The silicone shell of nanohybrids was not destroyed after 3 h of incubation, but partially biodegraded after 12 h of incubation, and completely degraded after 24 h of incubation. Moreover, the nanohybrids achieved satisfactory photodynamic, photothermal and chemotherapeutic outcomes, which nearly ablate the tumor under laser irradiation after five treatments. In addition, there has been report on the use of MONs and tetrasulfonate (-S-S-S-S-) for various therapeutic approaches. Chen et al designed new biodegradable mesoporous organic silica nanosheets doped with copper sulfide, which were used for co-treatment of chemotherapy and thermotherapy.<sup>60</sup> Tetrasulfide (-S-S-S-S-) was incorporated into the framework of silica nanosheets to achieve on-demand release of chemotherapeutics at tumor sites while it could achieve the degradation of MONs. The nanosheets were investigated in PBS with different GSH concentrations (0, 5, or 10 mM) for 14 d. When the concentration of GSH was increased to 5 mM, the structure of the nanosheets did not change significantly, but when the concentration was 10 mM, except for only small parts of the structure of the nanosheets, most of the nanosheets were destroyed.

## Periodic Mesoporous Organosilica

Bridged silsesquioxane (BS) nanoparticles were initiated by Shea's team and Brinker's team and had been studied in depth around the world in the preceding decades.<sup>67,68</sup> Silsesquioxane materials that showed ordered mesopores were called periodic mesoporous organosilica (PMO), which was obtained by the sol-gel process from organo-bridged alkoxysilanes in the presence of structure-directing agents.<sup>69</sup> Researchers have a long history of bridged organic groups such as ethyl (-CH<sub>2</sub>-CH<sub>2</sub>-), vinyl (-CH=CH-), ethynyl (-C≡C-), phenyl (-C<sub>6</sub>H<sub>4</sub>-), etc., into the silsesquioxane framework to study their degradation.<sup>70,71</sup> After introducing these groups, the silsesquioxane skeleton was more resistant to hydrolysis in PBS, and the degree of degradation was very slow with only 2% in 15 d. However, the silsesquioxane bridged by disulfide bond (-S-S-),<sup>72</sup> thioether bond (-S-S-S-),<sup>73,74</sup> and amide bond (-CO-NH-)<sup>75</sup> can be degraded through redox and enzymatic reactions to achieve rapid degradation. This degradation behavior is similar to that of bridged alkoxysilanes. Therefore, there is no elaboration here.

Compared with non-covalent organic doping, the degradation process of mesoporous organosilica nanoparticles and periodic mesoporous organosilica are more controllable and more in line with the characteristics of intelligent degradation. Mesoporous organosilica nanoparticles and periodic mesoporous organosilica mainly responds to oxidation-reduction reactions and enzyme reactions to achieve degradation through disulfide bond (-S-S-), sulfide bond (-S-S-S-S-), diselenide bond (-Se-), amide bond (-CO-NH-) to form a multifunctional degradable system, which may become the forefront of degradable MSNs.

## Degradation of MSNs by Metal Doping

The Si-O-Si framework of MSNs is relatively stable and difficult to degrade. According to the characteristics that the tumor microenvironment (TME) is weakly acidic and contains a high concentration of reducing substances, metal (M) ions are doped to a Si-O-M skeleton structure or metal oxides are formed in the skeleton gap.<sup>76</sup> Under acidic or reducing conditions, through the dissolution of metal ions or the dissolution characteristics of metal oxides, the Si-O-Si framework of MSNs gradually shows cracks, and further become sites for MSNs degradation, promoting collapse and degradation of the Si-O-Si framework. In addition, it had also been reported that metal and non-metal composite-doped MSNs could achieve the purpose of degradation.<sup>77</sup> Herein, the paper will introduce single metal-doped MSNs, multiple metal-doped MSNs, and metal and non-metal composite-doped MSNs to regulate the degradation of silica skeleton. Degradation trends at different times of metal and/or non-metal doped MSNs are listed in Table 2.

**Table 2** Degradation Trend at Different Time of Metal and/or Non-Metal Doped MSNs by TEM/SEM

Metal Elements/Non-metal Elements	Metal Oxide/Metal Ion	Degradation Trend at Different Time	Ref.
Iron	Fe <sup>3+</sup> (iron ethoxide)	Only irregular solid fragments were observed in FBS after 7 d.	[78]
Manganese	Mn <sup>2+</sup> (manganese sulfate monohydrate)	Ultra-small particles with a size of approximately 6 nm were observed under the conditions of 10 mM GSH and pH 5.0 after 24 h.	[79]
Calcium	CaO	The number of macropores showed a decrease within 3 d. Additionally, the number of mesopores exhibited a decrease over a longer duration of time.	[80]
	Ca <sup>2+</sup> (hydroxyapatite)	The material was observed to break and degrade into smaller aggregated nanoparticles at pH 6.0, and it was completely destroyed at pH 4.5 after 12 h.	[81]
Manganese+ Iron	Mn <sup>2+</sup> (manganese silicate) Fe <sub>3</sub> O <sub>4</sub>	The material underwent gradual degradation over time, and a significant amount of Fe <sub>3</sub> O <sub>4</sub> was exfoliated and could be degraded in the presence of pH 5.5 or 10 mM GSH within 2 h.	[82]

(Continued)

**Table 2** (Continued).

Metal Elements/Non-metal Elements	Metal Oxide/Metal Ion	Degradation Trend at Different Time	Ref.
Calcium+ Zinc	Ca <sup>2+</sup> (calcium chloride anhydrous) ZnO	The particles were completely undetectable in pH 5.0 PBS, and it was difficult to find any remaining undegraded particles in the co-culture of MSCNs and 4T1 cells after 7 d.	[83]
Copper+ Iron	Cu <sup>2+</sup> (copper nitrate trihydrate) Fe <sup>3+</sup> (iron nitrate nonahydrate)	The material exhibited a high degree of degradability in pH 5.0 PBS, and after being cultured in pH 7.4 PBS for 3 d, it showed slight porosity.	[84]
Zinc+ Gadolinium +Chromium+ Stannum +Manganese	Zn <sup>2+</sup> (zinc acetate dihydrate) Ga <sup>3+</sup> (gallium nitrate solution) Cr <sup>3+</sup> (chromium acetate) Sn <sup>4+</sup> (stannum chloride) Mn <sup>2+</sup> (manganese sulfate hydrate)	The material remained stable in a neutral environment, but significant changes were observed of incubation in pH 5.5 PBS and 10 mM GSH after 8 h.	[85]
Selenium + Bismuth	Se, selenium Bi <sup>3+</sup> (bismuth nitrate pentahydrate)	The material was completely degraded into very small nanoparticles at pH 6.5, while it showed slower degradation at pH 7.4 after 48 h.	[77]

### Single Metal Doping

In terms of single metal-doped MSNs, the effects of iron (Fe),<sup>78,86</sup> manganese (Mn),<sup>79,87–89</sup> calcium (Ca)<sup>80,81,90</sup> on the degradation of MSNs were mainly introduced. A study explored exposing Fe<sup>3+</sup> doped silica nanoshells to three small molecule chelatings to test whether the removal of Fe<sup>3+</sup> from the silica nanoshell structure would facilitate its degradation (Figure 3A).<sup>78</sup> The Fe<sup>3+</sup> content was measured by inductively coupled plasma optical emission spectroscopy (ICP-OES) and 57%, 39%, and 42% of Fe<sup>3+</sup> was removed after three small molecule chelating agents acted on the nanoshells for 24 h. It could be seen that with the removal of Fe<sup>3+</sup>, the nanoshell wall became thinner, and the structure collapsed in PBS. Fe<sup>3+</sup> doped silica nanoshells were difficult to find any nanoshells after 7 d (Figure 3B), and only irregular solid fragments could be seen.

Tang et al prepared folic acid-modified manganese-doped MSNs.<sup>87</sup> The manganese-oxygen bond (-Mn-O-) in MSNs was easily reduced by GSH. The cumulative release of Mn and Si reached the maximum percentages of 99.86±3.05% and 94.92±3.48% after 14 d in pH 5.0 with 10 mM GSH. However, the structure of manganese-doped MSNs remained relatively intact under the condition of GSH-free and pH 7.4 for 7 d. Similarly, Hao et al prepared a novel degradable and pH-responsive mesoporous silica nanoparticles/hydroxyapatite composites drug carrier by uniformly adding calcium salts to silica nanoparticles (Figure 3C).<sup>81</sup> TEM analysis showed that the nanoparticles composites became fragmentation in acid buffer solution (pH 5.0) for 12 h (Figure 3D). The degradable characteristics of the nanoparticles composites samples in pH 4.5 and 6.0 were also studied. It could be found from the TEM image that when processed in buffer solution of pH 6.0, the nanoparticles composites nanospheres were degraded into slightly large aggregated nanoparticles. When the pH was further reduced to 4.5, the nanoparticles composites sample was destroyed into small particles (Figure 3D). It indicated that the degradation of the nanoparticles composites was acid-responsive.

### Multiple Metal Doping

Multiple metal-doped MSNs adopt two forms: first, one metal was doped in the silica network framework, and the other was used to block the pores of MSNs, which reduced the leakage of drugs.<sup>82,83</sup> Second, multiple metals were co-doped in the framework of silica. Both methods could serve the purpose of degrading MSNs.

Sun et al prepared a responsive biodegradable manganese silicate nano-platform for dual-mode magnetic resonance imaging (MRI) guided cancer combination therapy based on TME.<sup>83</sup> Iron oxide (Fe<sub>3</sub>O<sub>4</sub>) nanoparticle modified on the surface of manganese silicate nano-platform could effectively block the pores of manganese silicate nano-platform and reduce the leakage of anticancer drugs under physiological conditions. Manganese silicate nano-platform had a good response to TME with weak acidity and high GSH condition. It was also an excellent T1-MRI contrast agent and suitable for drug delivery.<sup>88,89</sup> It could be seen from TEM that the structure of manganese silicate nano-platform could be



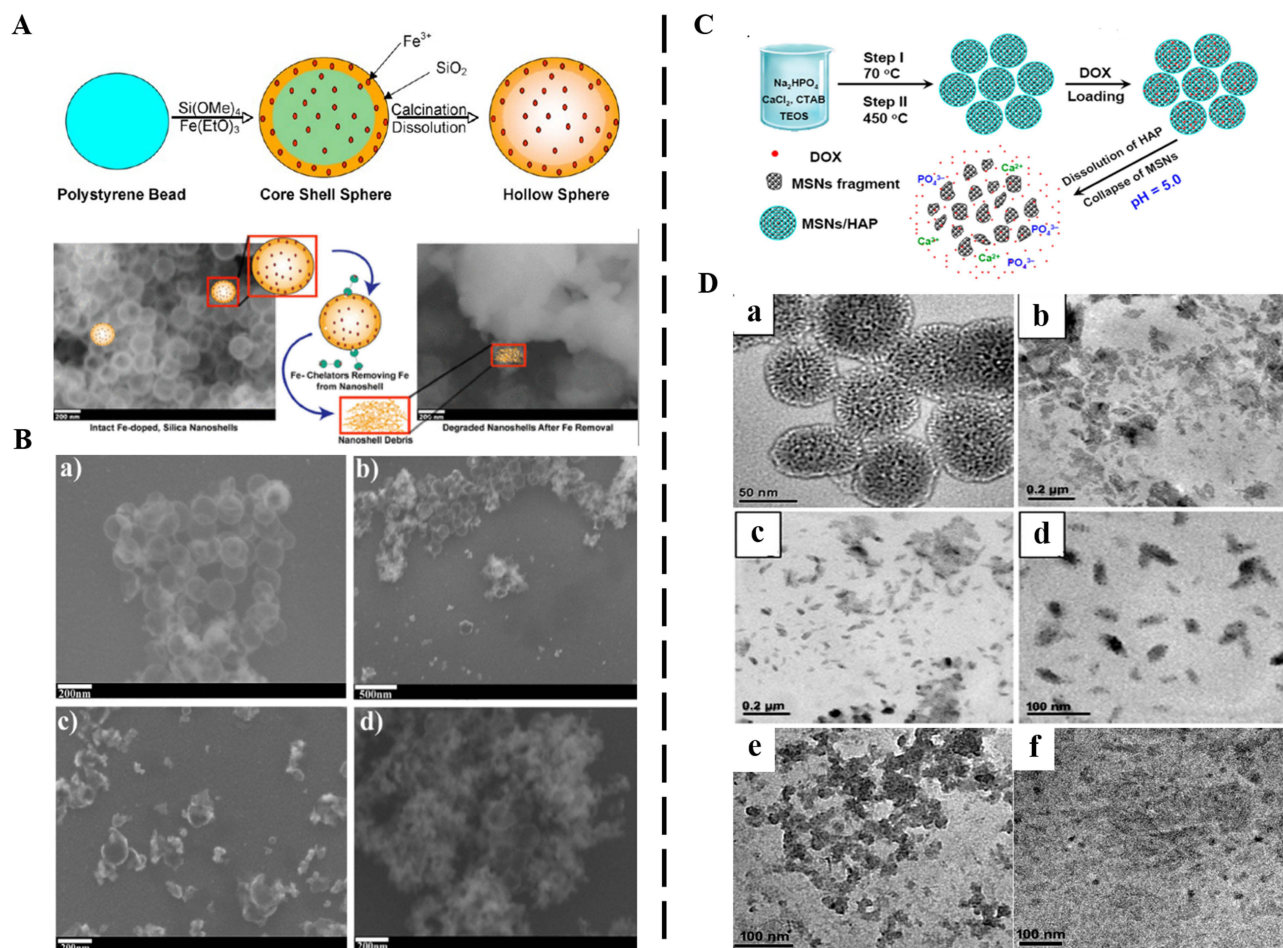


**Figure 3** Single metal doped MSNs for degradation.

**Notes:** (A) Synthesis and degradation process of Fe-doped silica nanoshells. (B) The collapse of Fe-doped silica nanoshell structure, imaged by SEM, as iron is removed, via deferiprone chelation, over 0 (a), 1 (b), 3 (c), and 7 d (d). Reprinted from Pohaku Mitchell KK, Liberman A, Kummel AC et al. Iron (III)-doped, silica nanoshells: a biodegradable form of silica. *J. Am. Chem. Soc.* 2012;134(34): 13,997–14,003. Copyright 2012 with permission from American Chemical Society.<sup>78</sup> (C) Schematic illustration of the synthesis, drug loading, and degradation process of the nanoparticles composites. (D) TEM images of the nanoparticles composites sample after degradation in acid buffer solution (pH 5.0) for (a) 0 h, (b) 4 h, (c) 12 h, and in acid buffer solution at (e) pH 6.0 and (f) pH 4.5 for 12 h. Reprinted from Hao XH, Hu XX, Zhang CM et al. Hybrid mesoporous silica-based drug carrier nanostructures with improved degradability by hydroxyapatite. *ACS Nano.* 2015;9(10):9614–9625. Copyright 2015 with permission from American Chemical Society.<sup>81</sup>

biodegraded gradually with time, and a large amount of exfoliated Fe<sub>3</sub>O<sub>4</sub> could be removed under the condition of 5.5 pH or 10 μM GSH within 2 h (Figure 4A). Further co-doping of two or more metals provided a reliable and important method to ensure the degradability of silica-based nanoparticles was reported by Liu et al.<sup>84</sup> They prepared mesoporous silica-based, bimetal-doped, biodegradable Janus-type (spherical ellipsoid) nanoreactors by arranging two different transition metals in the silica wall (Figure 4B). The nanoreactor was created by adding two different transition metals (Cu<sup>2+</sup> and Fe<sup>3+</sup>) to the silica wall using a simple one-step method. Degradation of the nanoreactors was observed for 3 d in pH 7.4 or pH 5.0. A high degree of degradability was present in pH 5.0, while the nanoreactors were only slightly porous after being cultured in pH 7.4. Therefore, the doping of two metal species into the silica wall will increase the function of acid response.<sup>85</sup>

### Metal and Non-Metal Composite Doping

Metal and non-metal composite doped-MSNs have great advantages in degradation. Zheng et al prepared a responsive biodegradable selenium-silica nanoparticle doped bismuth nanocomposite.<sup>77</sup> The nanocomposite was dispersed in PBS with different pH (6.5 and 7.4) to evaluate the degradation behavior. When the pH was 6.5, the complete structure of the nanocomposite appeared to crack at 4 h. More cracks and hollow holes appeared in the pipeline. After 48 h, the nanocomposite was completely degraded into tiny nanoparticles. The degradation rate of the nanocomposite in pH 7.4

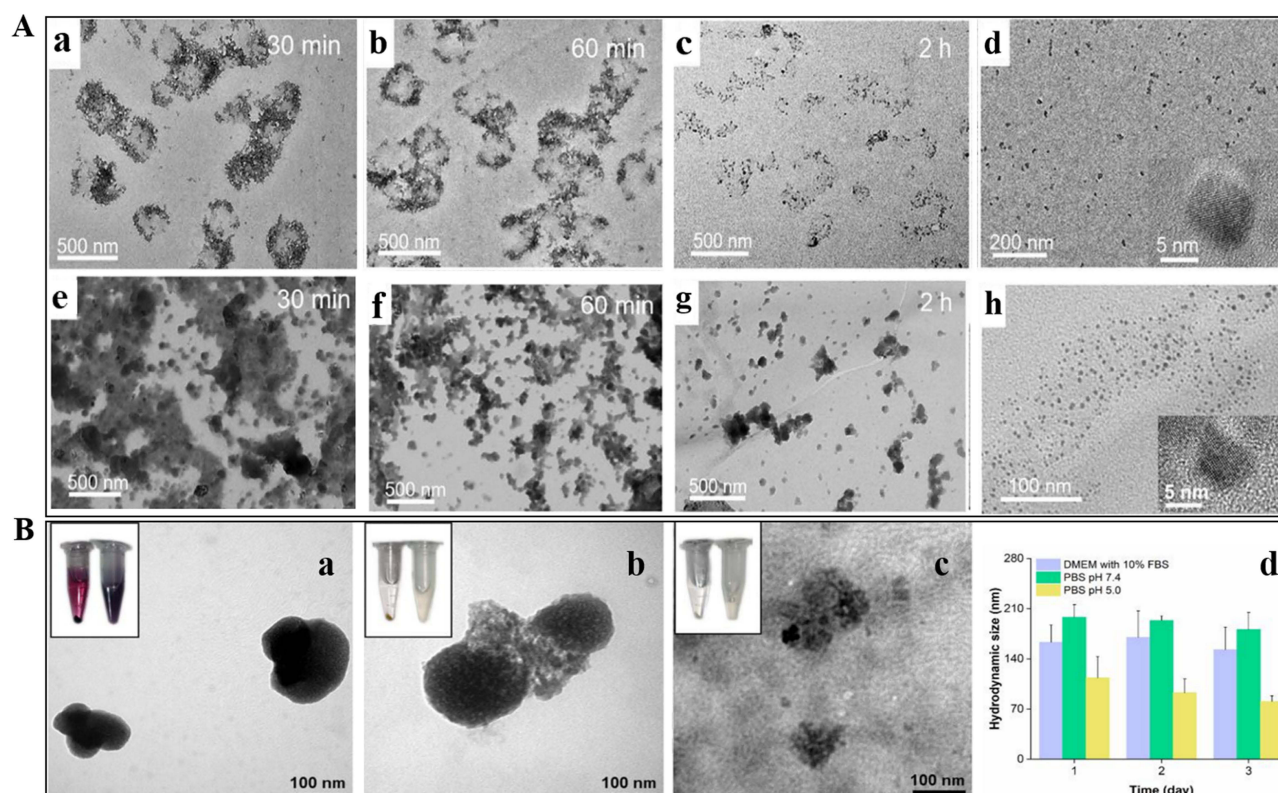


**Figure 4** Multiple metals doped MSNs for degradation.

**Notes:** (A) The Biodegradable behavior of Fe<sub>3</sub>O<sub>4</sub>-manganese silicate nano-platform at pH 5.5 over time: (a) 30 min, (b) 60 min, and (c) 2 h. (d) Exfoliated Fe<sub>3</sub>O<sub>4</sub> nanocrystals in solution. And the Biodegradable behavior of Fe<sub>3</sub>O<sub>4</sub>-manganese silicate nano-platform with 10 μM GSH over time: (e) 30 min, (f) 60 min, and (g) 2 h. (h) Exfoliated Fe<sub>3</sub>O<sub>4</sub> nanocrystals in solution. Reprinted from Sun X, Zhang GL, Du RH et al. A biodegradable MnSiO<sub>3</sub>@Fe<sub>3</sub>O<sub>4</sub> nanoplateform for dual-mode magnetic resonance imaging guided combinatorial cancer therapy. *Biomaterials*. 2019;194:151–160. Copyright 2019 with permission from Elsevier.<sup>83</sup> (B) In vitro degradation of Cu-Fe-MSNs in DMEM with 10% FBS (a), and PBS pH-7.4 (b) and pH-5.0 (c). Hydrodynamic sizes of Cu-Fe-MSNs in DMEM with 10% FBS, and PBS at pH-7.4 as well as pH-5.0 (d). Reprinted from Liu CG, Han YH, Zhang JT et al. Rerouting engineered metal-dependent shapes of mesoporous silica nanocontainers to biodegradable Janus-type (sphero-ellipsoid) nanoreactors for chemodynamic therapy. *Chem Eng J*. 2019;370:1188–1199. Copyright 2019 with permission from Elsevier.<sup>84</sup>

was slower than that in pH 6.5. This indicated that the nanocomposite has an acid-responsive function. Moreover, the nanocomposite could be degraded into less than 6 nm particles that could be excreted through metabolic pathways to avoid long-term toxicity.<sup>91</sup>

The degradation of metal doped MSNs mainly responds to the tumor microenvironment, and most of them achieve rapid degradation under acidic and GSH reduction conditions. Similarly, metal doping also has the characteristics of controllable and intelligent degradation, and can be widely used in the study of anti-tumor diseases.

## The Biodistribution of MSNs in vivo

It is known that most MSNs tend to exhibit high uptake in the RES of the liver and spleen.<sup>92</sup> If such a substantial number of nanoparticles reside in the tissues/organs and cannot undergo further degradation or excretion, it may cause cytotoxicity and other side effects. To best minimize toxicity and/or collateral effects, MSNs should either be degraded in situ into truly non-cytotoxic subcomponents or be cleared from the body, once it has served their diagnostic/therapeutic purpose. For the clearance of MSNs in vivo, only knowing where the biodistribution of MSNs in the body can govern their clearance.<sup>93–95</sup> He et al evaluated the biodistribution and urinary excretion of MSNs by intravenous injection in ICR mice in vivo.<sup>93</sup> The results indicated that MSNs distributed mainly in the liver and spleen (Figure 5A). The PEGylated MSNs of smaller particle size possessed longer blood-circulation lifetime, and were more slowly biodegraded and correspondingly had a lower excreted amount of degradation products in the urine (Figure 5A). In another study, Huang et al designed short/long rod-shaped (aspect ratios, 1.5, 5) fluorescein isothiocyanate MSNs, and modified them with PEG to track the biodistribution of MSNs after intravenous injection and used ICP-OES to analyze the Si content in organs in vivo.<sup>94</sup> The biodistribution of organs



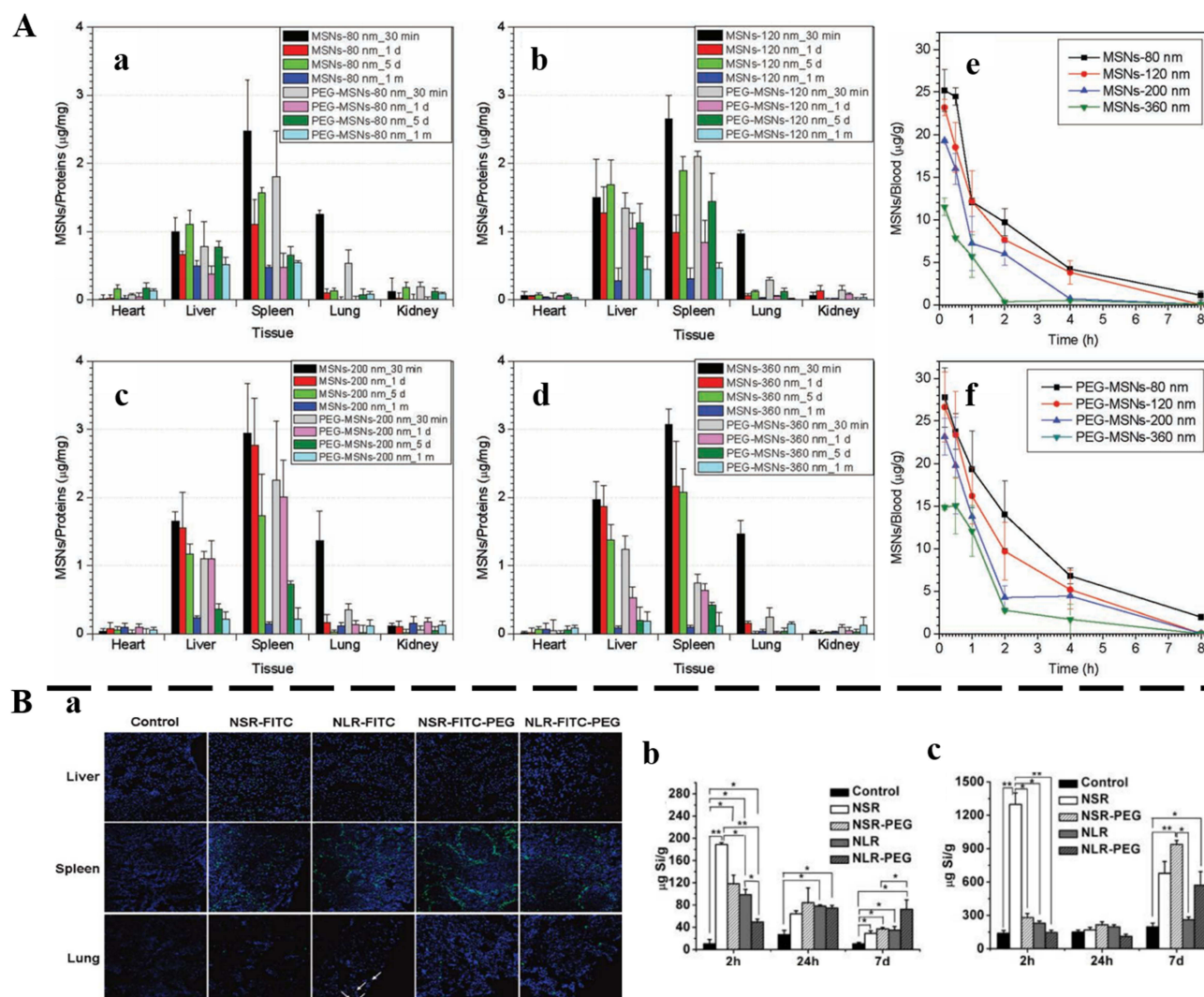


**Figure 5** The distribution of MSNs in vivo.

**Notes:** (A) Biodistribution of 80 nm (a), 120 nm (b), 200 nm (c), and 360 nm (d) MSNs and PEG-MSNs in heart, liver, spleen, lung, and kidney at different times. Pharmacokinetic processes of different particle sizes MSNs (e) and PEG-MSNs (f). Reprinted from He QJ, Zhang ZW, Gao F et al. In vivo biodistribution and urinary excretion of mesoporous silica nanoparticles: effects of particle size and PEGylation. *Small*. 2011;7(2):271–280. Copyright 2011 with permission from Wiley.<sup>93</sup> (B) Biodistribution of different shaped and PEGylated MSN-FITC in liver, spleen, and lung (a). ICP-OES quantitative analysis of the Si contents of different shaped and PEGylated MSNs in urine and feces. \*,  $p < 0.05$ ; \*\*,  $p < 0.01$ . Reprinted from Huang XL, Li LL, Liu TL et al. The shape effect of mesoporous silica nanoparticles on biodistribution, clearance, and biocompatibility in vivo. *ACS Nano*. 2011;5(7):5390–5399. Copyright 2011 with permission from American Chemical Society.<sup>94</sup>

showed that intravenous MSNs mainly existed in the liver, spleen, and lungs (Figure 5B), and significantly impacted the shape of particles. The liver exhibited a higher propensity for retaining short rod-shaped MSNs, whereas long rod-shaped MSNs tended to distribute within the spleen. After PEG modification, the content of MSNs with two aspect ratios was higher in the spleen and lung. At 2 h, 24 h, and 7 d after the injection, the Si content of each organ was found to decrease significantly over time (Figure 5B). In addition, the clearance rate of MSNs is primarily related to the particle shape, where short-rod MSNs have a more rapid clearance rate than long-rod MSNs in both excretion routes. It can be seen from the above cases that MSNs are mainly distributed in the liver and spleen, and excreted by the kidney.

## The Clearance of MSNs

In recent years, the clearance of MSNs has attracted extensive interest among researchers.<sup>13–15,28,29,36,96</sup> MSNs are often regarded as extraneous substance by immune system, which may lead to toxicity issues. After systemic administration,

MSNs are captured by the RES, including liver and spleen with slow clearance and low efficiency.<sup>97</sup> Long term retention of MSNs in the liver and spleen can trigger the aggregation behavior, leading to potential toxicity issues.<sup>98–102</sup>

Controlling the aggregation of MSNs during blood circulation is a crucial consideration in the development of nanodrugs. The formation of aggregates of MSNs can potentially cause embolism, severely limiting their in-vivo applications.<sup>103–105</sup> The presence of aggregates of MSNs has a profound impact on their biodistribution within the body. Typically, MSNs that exhibit strong aggregation tendencies are predominantly found in organs such as the liver, spleen, or other reticuloendothelial organs. To mitigate the aggregation of MSNs, enhance their physiological stability, and improve biocompatibility, diverse clearance strategies have been devised. Adjusting the physical attributes of MSNs, including their morphology, surface functional groups, surface charge, and size, plays a pivotal role in influencing the clearance rate of MSNs, making it a crucial strategy for effective clearance. Most importantly, only by understanding the clearance mechanism can we better achieve the clearance of MSNs. Therefore, this paper focuses on mechanisms of clearance and adjusting physical parameters of MSNs.

## Mechanisms of Clearance of MSNs

It is known that MSNs are mostly excreted through the renal pathway following systemic administration, and the clearance process involves renal filtration, where MSNs are eliminated through the kidneys and subsequently excreted via the bladder in the form of urine. Furthermore, MSNs can undergo clearance via the hepatobiliary pathway, where they are excreted from the liver into the intestine and ultimately eliminated through feces.<sup>106</sup> Nevertheless, part of the MSNs can reside relatively long in the body. In some studies, particles were still detected in the liver and spleen up to 8 weeks after injection. It's because MSNs are trapped by the RES, causing them to accumulate in the liver and spleen.<sup>106,107</sup> The general scheme for MSNs clearance is through three main mechanisms: renal, hepatobiliary, and RES (Figure 6).<sup>108</sup>

### Renal Clearance

Irrespective of the mode of entry into the blood, MSNs after the final degradation is lower than the renal clearance threshold (6 nm), they can be cleared by the kidney.<sup>109,110</sup> Understanding the renal clearance of MSNs is the basis of toxicity evaluation and in vivo application of MSNs. The modes of renal clearance include glomerular filtration, tubular secretion, and tubular reabsorption, among which glomerular filtration directly affects the renal clearance capacity. The glomerulus is composed of three layers: endothelial fenestrae, the glomerulus basement membrane (GBM), and the

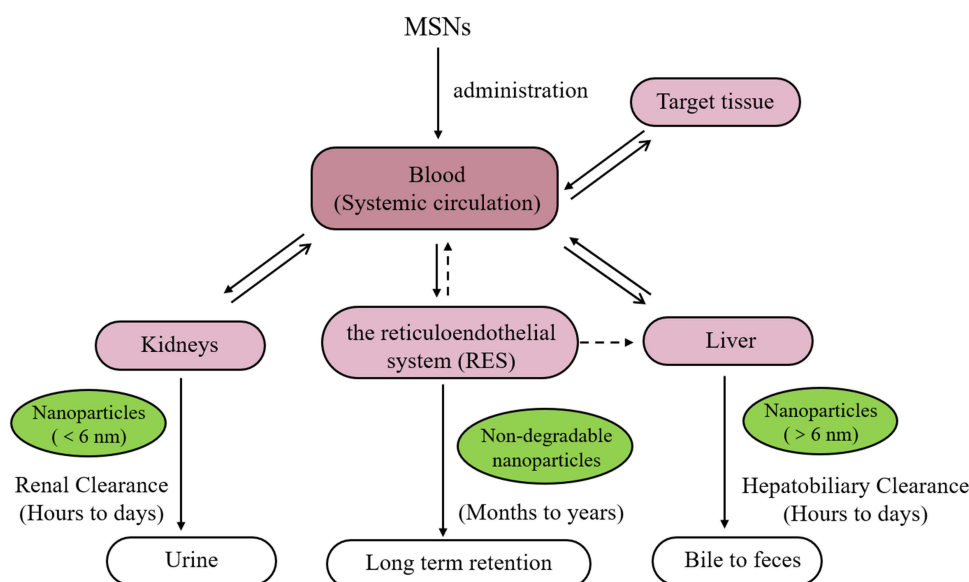


**Figure 6** The schematic of MSNs clearance pathways.

**Notes:** Reprinted from Yu MX, Zheng J. Clearance pathways and tumor targeting of imaging nanoparticles. *ACS Nano*. 2015;9(7):6655–6674. Copyright 2015 with permission from American Chemical Society.<sup>108</sup>



narrow gaps formed by the interdigitating podocyte processes in the renal filtration system. The size of renal clearance of MSNs largely depends on the narrow gaps in the renal filtration system. MSNs after degradation less than 6 nm in size have greater renal clearance than MSNs larger than 8 nm.<sup>28</sup> Similarly, the surface charge also affects the clearance rate of MSNs. Positively charged particles clear better than negatively or neutral counterparts.<sup>111</sup> In addition, the shape of MSNs is an additional important factor affecting renal filtration due to the rectangular shape of the slits within the GBM. Large linear-structured MSNs with a width less than the kidney filtration threshold can also be filtered through the kidneys. To briefly summarize, owing to the unique structure of the glomerular capillaries, renal ultrafiltration depends on particle size, surface charge, and shape. It should also be noted that several studies exist showing that MSNs with sizes significantly larger than 8 nm can be cleared via the urine.<sup>112,113</sup> Therefore, the mechanism of renal clearance needs further study.

## Hepatobiliary Clearance

Since the metabolism and clearance of foreign materials are major functions of the liver, MSNs that cannot be cleared by the renal system will eventually be processed in the liver. There is evidence that MSNs are preferentially deposited in the liver under systemic exposure, resulting in prolonged retention in some cases, and significant hepatotoxicity.<sup>114</sup> Understanding the structure and function of the hepatobiliary system aids in designing MSNs and is an effective means to avoid hepatotoxicity. The liver primarily consists of specialized cell types, including hepatocytes, phagocytic Kupffer cells, resident immune cells, and various specialized endothelial and epithelial cells.<sup>115</sup> Hepatocytes are key cells for MSNs clearance. Hepatocytes produce bile for the elimination of biological waste. Bile will travel through along the intrahepatic biliary tree from the liver to the duodenum or the gallbladder for temporary storage. Many stimuli will cause the bile to be excreted from the gallbladder and biliary tree into the intestine.<sup>116</sup>

The same as clearance through the kidney, hepatobiliary clearance is also considerably determined by their size, surface charge, and morphology.<sup>95</sup> The biophysical and chemical interactions between MSNs and biological components (biological liquid, protein, enzyme, etc.) also determine the clearance pathway of MSNs. The main pathway of MSNs clearance is through lysosome-related degradation.<sup>117</sup> Then mostly excreted from hepatocytes by emptying lysosomal contents into the bile.<sup>116</sup> According to their composition, MSNs will be excreted into the bile in varying degrees and transporting into the small intestine through the bile duct, eventually exiting in the form of feces.

## RES Clearance

The liver and spleen are regarded as a major part of the RES, and its resident macrophages, the Kupffer cells, are critical for the RES function.<sup>116</sup> Kupffer cells are positioned in liver sinusoids. Kupffer cells are tissue-resident macrophages that phagocytose and destroy foreign bodies and materials in the blood.<sup>118</sup> Once they enter macrophages, MSNs are processed and degraded in lysosomes where possible. Non-biodegradable MSNs will remain in intracellular until being sequestered by the spleen and liver, making its clearance significantly slower.<sup>27,119</sup> The RES is usually closely correlated with the long-term fate of MSNs in the organism, as MSNs captured by these cells persist for a long time in RES organs, especially if MSNs were not degraded.

## Clearance of MSNs by Adjusting Physical Parameters

The effective clearance of MSNs determines the balance between the activity and toxicity of MSNs, which is also a prerequisite for the application of MSNs in vivo.<sup>28,29,36,92</sup> The clearance of MSNs can be achieved by adjusting the adjusting physical parameters, such as particle size, shape, surface charge, and surface functionality.

He et al designed a size-shrinkable MSN-based nanocarrier, which used acid to trigger particle size changes to jointly achieve effective tumor accumulation, followed by deep tumor penetration and rapid clearance from the body.<sup>112</sup> The silicon content of size-shrinkable MSN-based nanocarriers and ordinary MSN-based nanocarriers in urine and feces was measured by ICP-OES. The results showed that more than 49.25% of size-shrinkable MSN-based nanocarriers was excreted out of the body by urine and feces within 72 h, and thereinto, the amount of excreted Si in urine and feces reached 42.73% and 6.52% ID, respectively (Figure 7A). That's because size-shrinkable MSN-based nanocarriers could be cleared from the body due to pH-induced particle size shrinkage. In addition, shape modification can influence the

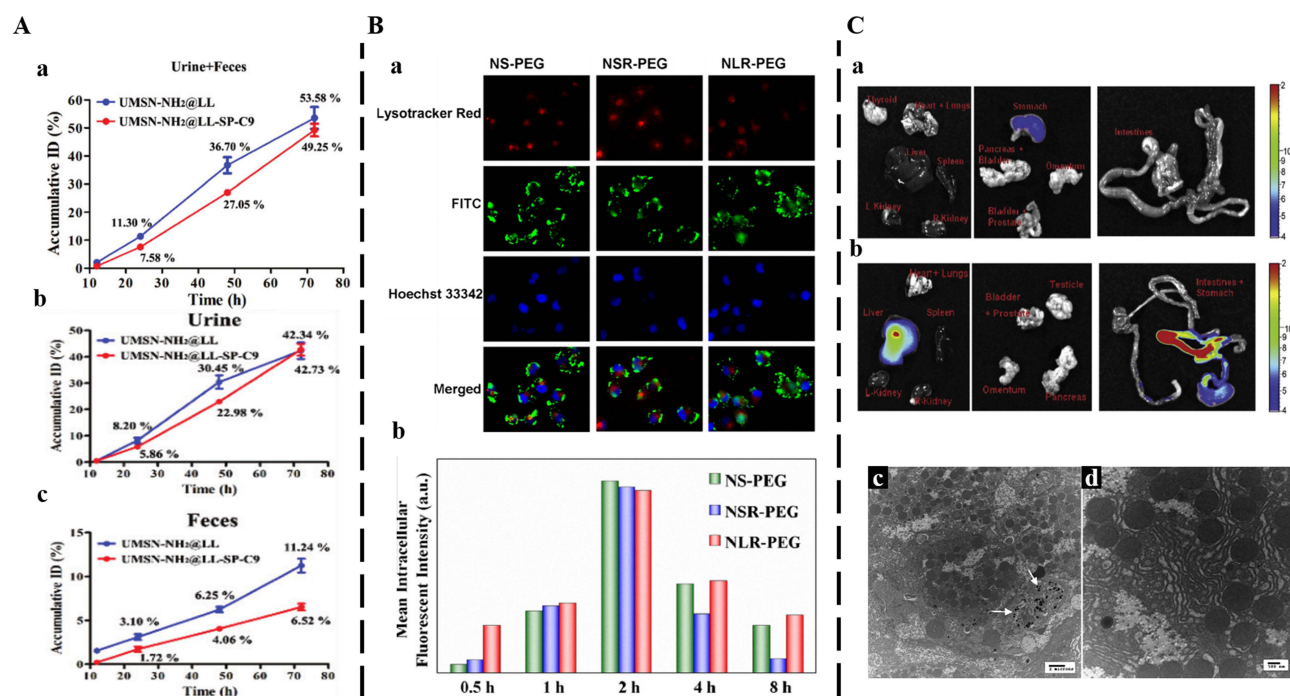


**Figure 7** Clearance of MSNs by varying physical parameters.

**Notes:** (A) Excretion profiles of the Si element in the urine and feces (a), urine (b), or feces (c) after treatment with ordinary MSN-based nanocarriers and size-shrinkable MSN-based nanocarriers. Reprinted from He YJ, Fan XY, Wu XZ et al pH-Responsive size-shrinkable mesoporous silica-based nanocarriers for improving tumor penetration and therapeutic efficacy. *Nanoscale*. 2022;14(4):1271–1284. Copyright 2022 with permission from The Royal Society of Chemistry.<sup>112</sup> (B) Fluorescent microscopy images of HeLa cells after treatment with NS-PEG, NSR-PEG, and NLR-PEG. Flow cytometry results show intracellular fluorescence intensity of NS-PEG, NSR-PEG, and NLR-PEG in HeLa cells. Reprinted from Hao N, Li L, Zhang Q et al. The shape effect of PEGylated mesoporous silica nanoparticles on cellular uptake pathway in HeLa cells. *Micropor. Mesopor. Mat.* 2012;162:14–23. Copyright 2012 with permission from Elsevier.<sup>120</sup> (C) Fluorescence images of isolated organs from control mouse (a) and administration mouse after treatment with positively charged MSNs (b). Excretion status of 10 min (2  $\mu$ m scale-bar) (c) and (d) 3 d (500 nm scale-bar) after treatment with positively charged MSNs. Reprinted from Souris JS, Lee CH, Cheng SH et al. Surface charge-mediated rapid hepatobiliary excretion of mesoporous silica nanoparticles. *Biomaterials*. 2010;31(21):5564–5574. Copyright 2010 with permission from Elsevier.<sup>122</sup>

clearance behavior of MSNs. The clearance of MSNs with different shapes in vivo is more reflected in the interaction between MSNs and phagocytes in the RES. For a sharpened understanding of intracellular clearance fates of different shapes of MSNs, the cellular uptake kinetics, the intracellular uptake, and endocytosis mechanism, should be paid appropriately consideration. Hao et al prepared three different kinds of fluorescent MSNs (aspect ratio=1, 2, and 4).<sup>120</sup> The results showed that the uptake kinetics and endocytosis pathway of three different shaped MSNs-PEG were shape-dependent (Figure 7B). The long-rod MSNs-PEG (NLR-PEG) showed higher intracellular retention than the short-rod MSNs-PEG (NSR-PEG) and spherical MSNs-PEG (NS-PEG) for almost 8 h (Figure 7B). The NSR-PEG showed the lowest intracellular amount, especially with prolonged incubation time. Spherical particles preferred to be internalized via the clathrin-mediated pathway, whereas MSNs with larger aspect ratios favored being internalized via the caveolae-mediated pathway, which could explain their different uptake kinetics and endocytosis mechanism. This provides a theoretical basis for the accumulation in the RES and in vivo clearance of different shapes of MSNs. Furthermore, the accumulation in the RES was due to the adsorption of serum proteins onto nanoparticles, which is why MSNs are often functionalized with hydrophilic polymers such as PEG.<sup>121</sup> The charge also is an important factor affecting the clearance of MSNs in vivo. Souris et al synthesized highly positively charged MSNs that displayed rapid hepatobiliary excretion.<sup>122</sup> The fraction with a significantly high positive charge (+34.4 mV at pH 7.4) was promptly eliminated from the liver and transported to the gastrointestinal tract (Figure 7C). In contrast, the fraction with a lower negative charge (−17.6 mV at pH 7.4) remained localized within the liver. In addition, the affinity of serum proteins for MSNs, which is influenced by their charge, played a crucial role in facilitating the hepatobiliary excretion of MSNs (Figure 7C). Consequently, by controlling the surface charge, it was possible to regulate the duration of nanoparticle residence

in vivo. The mechanism may be that the surface-charged MSNs could adsorb serum proteins, thereby affecting the circulation, distribution, and excretion pathways of MSNs in vivo.

In addition, it was also reported that an ultrasmall porous MSNs (<6 nm) was capable of prolonged plasma half-life, attenuated the RES sequestration, and accelerated renal clearance.<sup>123</sup> Kim and coworkers reported a hyaluronic acid-integrated ultrasmall silica nanoparticles.<sup>124</sup> Hyaluronic acid having negative charges and ultrasmall porous MSNs showing strong optical absorbance in near-infrared windows could avoid phagocytosis of RES and aid in visualizing the targeted delivery. The absorption spectra of the collected urine showed that these nanoparticles could be cleared by urine from the body after the accumulation in the liver. Another study reported that a disulfide-bridged MONs also had great advantages in vivo clearance. Zhou et al designed a Janus-type upconverted MONs with loaded chlorin e6 for NIR-induced photothermal dynamic therapy.<sup>125</sup> Compared with non-degradable upconverted MSNs, the Janus-type upconverted MONs containing a disulfide-bridged silica framework improved chlorin e6 release from the tumor microenvironment and depleted glutathione inside cancer cells, thereby enhancing efficacy of photothermal dynamic therapy. More importantly, quantitative evaluation in a mouse model revealed higher clearance of upconverted MONs than that of upconverted MSNs, thus alleviating the persistence of nanomaterial in the body.

## Conclusion and Further Prospects

MSNs have been widely used in the field of drug delivery, while the long-term and non-specific accumulation is currently considered to be a key issue hindering its further application. Through some strategies, MSNs can be decomposed in vivo accelerating clearance and largely improving biosafety. This review systematically introduces various strategies for adjusting the degradation and clearance of MSNs. The content about the degradation of MSNs mainly introduces three aspects, including regulating physicochemical properties, doping non-covalent organic molecules, mesoporous organosilica nanoparticles and periodic mesoporous organosilica, and doping metal ions or metal oxides into the MSNs framework. Subsequently, we introduced the biodistribution of MSNs in vivo after degradation. In terms of clearance, the clearance mechanisms and clearance strategies by adjusting physical parameters were introduced.

A large number of experiments have demonstrated that MSNs can be well degraded and cleared by various strategies. Meanwhile, the targeting efficiency should not be compromised excessively by degradation and clearance. After achieving functional effects in the body, MSNs must be gradually excreted by the clearance pathway. Moreover, it is crucial to acknowledge the substantial disparities that exist in the degradation and clearance of MSNs between experimental media, cellular systems, and living organisms. While experiments conducted in solutions or cells allow for precise regulation of degradation and clearance rates, concerns regarding biodistribution and clearance kinetics become more prominent in the context of whole organisms. Nevertheless, the remarkable advancements made over the past decades, driven by exploratory research and discoveries, have propelled the remarkable growth of degradable and clearable MSNs. The significant outcomes obtained thus far demonstrate the immense potential of degradable and clearable MSNs in cancer treatment. Given these remarkable achievements, MSNs with adjustable degradation and clearance properties hold a promising future in the field of biomedical applications.

## Abbreviations

MSNs, mesoporous silica nanoparticles; FDA, Food and Drug Administration; SIF, simulated intestinal fluid; SBF, simulated body fluid; PBS, phosphate buffer solution; BSA, bovine serum albumin; RES, reticuloendothelial system; SGF, simulated gaussian fluid; TME, tumor microenvironment; Fe, iron; Mn, manganese; Ca, calcium; Bio-TEM, biological transmission electron microscope; ICP-OES, inductively coupled plasma optical emission spectroscopy; -Mn-O-, -oxygen bond-; GSH, glutathione; CaO, calcium oxide; SEM, scanning electron microscope; MRI, magnetic resonance imaging; Man, mannose; MONs, mesoporous organosilica nanoparticles; -S-S-, disulfide bond; -S-S-S-S-, sulfide bond; -Se-Se-, diselenide bond; -CO-NH-, amide bond; PMO, periodic mesoporous organosilica; DTT, dithiothreitol; BS, Bridged silsesquioxane; -CH<sub>2</sub>-CH<sub>2</sub>-, ethyl; -CH=CH-, vinyl; -C≡C-, ethynyl; -C<sub>6</sub>H<sub>4</sub>-, phenyl.

## Acknowledgments

This work is supported by the National Science Foundation of China (NO.82074027, NO.82104405), Natural Science Foundation of Zhejiang Province (NO.LZ21H280001).

## Disclosure

The authors declare no conflicts of interest.

## References

- Zhuang J, Chen S, Hu Y, et al. Tumour-targeted and redox-responsive mesoporous silica nanoparticles for controlled release of doxorubicin and an siRNA against metastatic breast cancer. *Int J Nanomed*. 2021;16:1961–1976. doi:10.2147/IJN.S278724
- Xu C, Lei C, Yu CZ. Mesoporous silica nanoparticles for protein protection and delivery. *Front Chem*. 2019;7:290. doi:10.3389/fchem.2019.00290
- Kankala RK, Han YH, Na J, et al. Nanoarchitected structure and surface biofunctionality of mesoporous silica nanoparticles. *Adv Mater*. 2020;32(23):1907035. doi:10.1002/adma.201907035
- Porrang S, Davaran S, Rahemi N, et al. How advancing are mesoporous silica nanoparticles? A comprehensive review of the literature. *Int J Nanomed*. 2022;17:1803–1827. doi:10.2147/IJN.S353349
- Croissant JG, Fatieiev Y, Almalik A, et al. Mesoporous silica and organosilica nanoparticles: physical chemistry, biosafety, delivery strategies, and biomedical applications. *Adv Healthc Mater*. 2018;7(4):1700831. doi:10.1002/adhm.201700831
- Igaz N, Béltéký P, Kovács D, et al. Functionalized mesoporous silica nanoparticles for drug-delivery to multidrug-resistant cancer cells. *Int J Nanomed*. 2022;17:3079–3096. doi:10.2147/IJN.S363952
- Lin J, Shi T, Wang Y, et al. Hybrid hydrogel loaded with chlorhexidine- $\beta$ -CD-MSN composites as wound dressing. *Int J Nanomed*. 2023;18:1725–1740. doi:10.2147/IJN.S401705
- Cui L, Liu W, Liu H, et al. Cascade-targeting of charge-reversal and disulfide bonds shielding for efficient DOX delivery of multistage sensitive MSNs-COS-SS-CMC. *Int J Nanomed*. 2020;15:6153–6165. doi:10.2147/IJN.S252769
- Blum AP, Kammeyer JK, Rush AM, et al. Stimuli-responsive nanomaterials for biomedical applications. *J Am Chem Soc*. 2015;137(6):2140–2154. doi:10.1021/ja510147n
- Alberti S, Soler-Illia GJAA, Azzaroni O. Gated supramolecular chemistry in hybrid mesoporous silica nanoarchitectures: controlled delivery and molecular transport in response to chemical, physical and biological stimuli. *Chem Commun*. 2015;51(28):6050–6075. doi:10.1039/c4cc10414e
- Nguyen TL, Choi Y, Kim J. Mesoporous silica as a versatile platform for cancer immunotherapy. *Adv Mater*. 2019;31(34):1803953. doi:10.1002/adma.201803953
- Fang Z, Li X, Xu Z, et al. Hyaluronic acid-modified mesoporous silica-coated superparamagnetic Fe<sub>3</sub>O<sub>4</sub> nanoparticles for targeted drug delivery. *Int J Nanomed*. 2019;14:5785–5797. doi:10.2147/IJN.S213974
- Chen Y, Chen HR, Shi JL. In vivo bio-safety evaluations and diagnostic/therapeutic applications of chemically designed mesoporous silica nanoparticles. *Adv Mater*. 2013;25(23):3144–3176. doi:10.1002/adma.201205292
- Hosseinpour S, Walsh LJ, Xu C. Biomedical application of mesoporous silica nanoparticles as delivery systems: a biological safety perspective. *J Mater Chem B*. 2020;8(43):9863–9876. doi:10.1039/d0tb01868f
- Lérida-Viso A, Estepa-Fernández A, García-Fernández A, et al. Biosafety of mesoporous silica nanoparticles; towards clinical translation. *Adv Drug Deliv Rev*. 2023;201:115049. doi:10.1016/j.addr.2023.115049
- Fortis SP, Batrinou A, Georgatzakou HT, et al. Effect of silica-based mesoporous nanomaterials on human blood cells. *Chem Biol Interact*. 2023;110784. doi:10.1016/j.cbi.2023.110784
- Liu TL, Li LL, Teng X, et al. Single and repeated dose toxicity of mesoporous hollow silica nanoparticles in intravenously exposed mice. *Biomaterials*. 2011;32(6):1657–1668. doi:10.1016/j.biomaterials.2010.10.035
- MacCuaig WM, Samykutty A, Foote J, et al. Toxicity assessment of mesoporous silica nanoparticles upon intravenous injection in mice: implications for drug delivery. *Pharmaceutics*. 2022;14(5):969. doi:10.3390/pharmaceutics14050969
- Choi HS, Liu WH, Misra P, et al. Renal clearance of quantum dots. *Nat Biotechnol*. 2007;25(10):1165–1170. doi:10.1038/nbt1340
- Bayda S, Hadla M, Palazzolo S, et al. Inorganic nanoparticles for cancer therapy: a transition from lab to clinic. *Curr Med Chem*. 2018;25(34):4269–4303. doi:10.2174/0929867325666171229141156
- Zou Z, He XX, He DG, et al. Programmed packaging of mesoporous silica nanocarriers for matrix metalloproteinase 2-triggered tumor targeting and release. *Biomaterials*. 2015;58:35–45. doi:10.1016/j.biomaterials.2015.04.034
- Du X, Kleitz F, Li XY, et al. Disulfide-bridged organosilica frameworks: designed, synthesis, redox-triggered degradation, and nanobiomedical applications. *Adv Funct Mater*. 2018;28(26):1707325–1707360. doi:10.1002/adfm.201707325
- Kempen PJ, Greasley S, Parker KA, et al. Theranostic mesoporous silica nanoparticles biodegrade after pro-survival drug delivery and ultrasound/magnetic resonance imaging of stem cells. *Theranostics*. 2015;5(6):631–642. doi:10.7150/thno.11389
- Yamada H, Urata C, Aoyama Y, et al. Preparation of colloidal mesoporous silica nanoparticles with different diameters and their unique degradation behavior in static aqueous systems. *Chem Mater*. 2012;24(8):1462–1471. doi:10.1021/cm3001688
- Yuan PY, Yang F, Liew SS, et al. Intracellular co-delivery of native antibody and siRNA for combination therapy by using biodegradable silica nanocapsules. *Biomaterials*. 2022;281:121376. doi:10.1016/j.biomaterials.2022.121376
- Yu LD, Chen Y, Lin H, et al. Magnesium-engineered silica framework for pH-accelerated degradation and DNase-triggered chemotherapy. *Small*. 2018;14(35):1800708. doi:10.1002/smll.201800708
- Bourquin J, Milosevic A, Hauser D, et al. Biodistribution, clearance, and long-term fate of clinically relevant nanomaterials. *Adv Mater*. 2018;30(19):1704307. doi:10.1002/adma.201704307
- Croissant JG, Fatieiev Y, Khashab NM. Degradability and clearance of silicon, organosilica, silsesquioxane, silica mixed oxide, and mesoporous silica nanoparticles. *Adv Mater*. 2017;29(9):1604634. doi:10.1002/adma.201604634
- Yang GB, Phua SZF, Bindra AK, et al. Degradability and clearance of inorganic nanoparticles for biomedical applications. *Adv Mater*. 2019;31(10):e1805730. doi:10.1002/adma.201805730
- Cheng YY, Jiao XY, Fan WP, et al. Controllable synthesis of versatile mesoporous organosilica nanoparticles as precision cancer theranostics. *Biomaterials*. 2020;256:120191–120209. doi:10.1016/j.biomaterials.2020.120191



31. Chen Y, Shi JL. Chemistry of mesoporous organosilica in nanotechnology: molecularly organic-inorganic hybridization into frameworks. *Adv Mater*. 2016;28(17):3235–3272. doi:10.1002/adma.201505147
32. Van PVD, Esquivel D, Canck ED, et al. Periodic mesoporous organosilicas: from simple to complex bridges; a comprehensive overview of functions, morphologies and applications. *Chem Soc Rev*. 2013;42(9):3913–3955. doi:10.1039/c2cs35222b
33. Du X, Li XY, Xiong L, et al. Mesoporous silica nanoparticles with organo-bridged silsesquioxane framework as innovative platforms for bioimaging and therapeutic agent delivery. *Biomaterials*. 2016;91:90–127. doi:10.1016/j.biomaterials.2016.03.019
34. Teng ZG, Su XD, Lee BH, et al. Yolk-shell structured mesoporous nanoparticles with thioether-bridged organosilica frameworks. *Chem Mater*. 2014;26:5980–5987. doi:10.1021/cm502777e
35. Fatieiev Y, Croissant JG, Alamoudi K, et al. Cellular internalization and biocompatibility of periodic mesoporous organosilica nanoparticles with tunable morphologies: from nanospheres to nanowires. *Chem Plus Chem*. 2017;82(4):631–637. doi:10.1002/cplu.201600560
36. Li LL, Liu TL, Fu CH, et al. Biodistribution, excretion, and toxicity of mesoporous silica nanoparticles after oral administration depends on their shape. *Nanomedicine*. 2015;11(8):1915–1924. doi:10.1016/j.nano.2015.07.004
37. Bindini E, Chehadi Z, Faustini M, et al. Following in situ the degradation of mesoporous silica in biorelevant conditions: at last, a good comprehension of the structure influence. *ACS Appl Mater Interfaces*. 2020;12(12):13598–13612. doi:10.1021/acsami.9b19956
38. Li H, Wu X, Yang B, et al. Evaluation of biomimetically synthesized mesoporous silica nanoparticles as drug carriers: structure, wettability, degradation, biocompatibility and brain distribution. *Mater Sci Eng C Mater Biol Appl*. 2019;94:453–464. doi:10.1016/j.msec.2018.09.053
39. Rosenbrand R, Barata D, Sutthavas P, et al. Lipid surface modifications increase mesoporous silica nanoparticle labeling properties in mesenchymal stem cells. *Int J Nanomed*. 2018;13:7711–7725. doi:10.2147/IJN.S182428
40. Desai D, Prabhakar N, Mamaeva V, et al. Targeted modulation of cell differentiation in distinct regions of the gastrointestinal tract via oral administration of differently PEG-PEI functionalized mesoporous silica nanoparticles. *Int J Nanomed*. 2016;11:299–313. doi:10.2147/IJN.S94013
41. Beck M, Mandal T, Buske C, et al. Serum protein adsorption enhances active leukemia stem cell targeting of mesoporous silica nanoparticles. *ACS Appl Mater Interfaces*. 2017;9(22):18566–18574. doi:10.1021/acsami.7b04742
42. Li C, Ge X, Li Y, et al. Modulation of release behaviors of methylene blue from degradable silica-methylene blue@octacalcium phosphate powders with different shell structures. *Colloid Surf A*. 2015;472:78–84. doi:10.1016/j.colsurfa.2015.02.041
43. Chen Z, Chen Z, Zhang A, et al. Electrospun nanofibers for cancer diagnosis and therapy. *Biomater Sci*. 2016;4(6):922–932. doi:10.1039/c6bm00070c
44. Wang A, Yang Y, Qi Y, et al. Fabrication of mesoporous silica nanoparticle with well-defined multicompartiment structure as efficient drug carrier for cancer therapy in vitro and in vivo. *ACS Appl Mater Interfaces*. 2016;8(14):8900–8907. doi:10.1021/acsami.5b12031
45. Hu X, Shi YN, Zhang P, et al. d-Mannose: properties, production, and applications: an overview. *Compr Rev Food Sci F*. 2016;15(4):773–785. doi:10.1111/1541-4337.12211
46. Li ZM, Yang Y, Wei HX, et al. Charge-reversal biodegradable MSNs for tumor synergetic chemo/photothermal and visualized therapy. *J Control Release*. 2021;338:719–730. doi:10.1016/j.jconrel.2021.09.005
47. Palanikumar L, Kim JM, Oh JY, et al. Hyaluronic acid-modified polymeric gatekeepers on biodegradable mesoporous silica nanoparticles for targeted cancer therapy. *ACS Biomater Sci Eng*. 2018;4(5):1716–1722. doi:10.1021/acsbiomaterials.8b00218
48. Yang Y, Wan J, Niu Y, et al. Structure-dependent and glutathione-responsive biodegradable dendritic mesoporous organosilica nanoparticles for safe protein delivery. *Chem Mater*. 2016;28(24):9008–9016. doi:10.1021/acs.chemmater.6b03896
49. Croissant JG, Fatieiev Y, Julfakyan K, et al. Biodegradable oxamide-phenylene-based mesoporous organosilica nanoparticles with unprecedented drug payloads for delivery in cells. *Chemistry*. 2016;22(42):14806–14811. doi:10.1002/chem.201601714
50. Moon H, Collanton RP, Monroe JI, et al. Evidence for entropically controlled interfacial hydration in mesoporous organosilicas. *J Am Chem Soc*. 2022;144(4):1766–1777. doi:10.1021/jacs.1c11342
51. Huang P, Chen Y, Lin H, et al. Molecularly organic/inorganic hybrid hollow mesoporous organosilica nanocapsules with tumor-specific biodegradability and enhanced chemotherapeutic functionality. *Biomaterials*. 2017;125:23–37. doi:10.1016/j.biomaterials.2017.02.018
52. Dang M, Li W, Zheng Y, et al. Mesoporous organosilica nanoparticles with large radial pores via an assembly-reconstruction process in bi-phase. *J Mater Chem B*. 2017;5(14):2625–2634. doi:10.1039/c6tb03327j
53. Teng ZG, Su XD, Zheng YY, et al. A facile multi-interface transformation approach to monodisperse multiple-shelled periodic mesoporous organosilica hollow spheres. *J Am Chem Soc*. 2015;137(24):7935–7944. doi:10.1021/jacs.5b05369
54. Lu J, Shi T, Shi C, et al. Thiol-disulfide exchange coordinates the release of nitric oxide and dexamethasone for synergistic regulation of intestinal microenvironment in colitis. *Research*. 2023;6:0204. doi:10.34133/research.0204
55. Zhang F, Chen F, Yang C, et al. Coordination and redox dual-responsive mesoporous organosilica nanoparticles amplify immunogenic cell death for cancer chemoimmunotherapy. *Small*. 2021;17(26):e2100006. doi:10.1002/smll.202100006
56. Wang K, Li X, Wang H, et al. Evaluation on redox-triggered degradation of thioether-bridged hybrid mesoporous organosilica nanoparticles. *Colloid Surf A*. 2021;608:125566. doi:10.1016/j.colsurfa.2020.125566
57. Yang Y, Lu Y, Abbaraju PL, et al. Stepwise degradable nanocarriers enabled cascade delivery for synergistic cancer therapy. *Adv Funct Mater*. 2018;28(28):1800706. doi:10.1002/adfm.201800706
58. Shao D, Li MQ, Wang Z, et al. Bioinspired diselenide-bridged mesoporous silica nanoparticles for dual-responsive protein delivery. *Adv Mater*. 2018;30(29):1801198. doi:10.1002/adma.201801198
59. Liu Y, Zhai SJ, Jiang XW, et al. Intracellular mutual promotion of redox homeostasis regulation and iron metabolism disruption for enduring chemodynamic therapy. *Adv Funct Mater*. 2021;31:2010390. doi:10.1002/adfm.202010390
60. Chen L, Meng X, Liu M, et al. Biodegradable mesoporous organosilica nanosheets for chemotherapy/mild thermotherapy of cancer: fast internalization, high cellular uptake, and high drug loading. *ACS Appl Mater Interfaces*. 2020;12(27):30234–30246. doi:10.1021/acsami.0c09735
61. Shao D, Zhang F, Chen F, et al. Biomimetic diselenide-bridged mesoporous organosilica nanoparticles as an X-ray-responsive biodegradable carrier for chemo-immunotherapy. *Adv Mater*. 2020;32(50):e2004385. doi:10.1002/adma.202004385
62. Xu J, Xu J, Shi T, et al. Probiotic-inspired nanomedicine restores intestinal homeostasis in colitis by regulating redox balance, immune responses, and the gut microbiome. *Adv Mater*. 2023;35(3):e2207890. doi:10.1002/adma.202207890

63. Yang Y, Chen F, Xu N, et al. Red-light-triggered self-destructive mesoporous silica nanoparticles for cascade-amplifying chemo-photodynamic therapy favoring antitumor immune responses. *Biomaterials*. 2022;281:121368. doi:10.1016/j.biomaterials.2022.121368
64. Meng Q, Meng J, Ran W, et al. Light-activated core-shell nanoparticles for spatiotemporally specific treatment of metastatic triple-negative breast cancer. *ACS Nano*. 2018;12(3):2789–2802. doi:10.1021/acsnano.7b09210
65. Chen X, Zhang Q, Li J, et al. Rattle-structured rough nanocapsules with in-situ-formed Gold nanorod cores for complementary gene/Chemo/photothermal therapy. *ACS Nano*. 2018;12(6):5646–5656. doi:10.1021/acsnano.8b01440
66. Cheng D, Ji Y, Wang B, et al. Dual-responsive nanohybrid based on degradable silica-coated gold nanorods for triple-combination therapy for breast cancer. *Acta Biomater*. 2021;128:435–446. doi:10.1016/j.actbio.2021.04.006
67. Zhao L, Vaupel M, Loy DA, et al. Photoresponsive hybrid materials: synthesis and characterization of coumarin-dimer-bridged polysilsesquioxanes. *Chem Mater*. 2008;20(5):1870–1876. doi:10.1021/cm702804r
68. Jiang YB, Xomeritakis G, Chen Z, et al. Sub-10 nm thick microporous membranes made by plasma-defined atomic layer deposition of a bridged silsesquioxane precursor. *J Am Chem Soc*. 2007;129(50):15446–15447. doi:10.1021/ja0773756
69. Croissant JG, Cattoen X, Wong MC, et al. Syntheses and applications of periodic mesoporous organosilica nanoparticles. *Nanoscale*. 2015;7(48):20318–20334. doi:10.1039/c5nr05649g
70. Tamanoi F, Chinnathambi S, Laird M, et al. Construction of boronophenylalanine-loaded biodegradable periodic mesoporous organosilica nanoparticles for BNCT cancer therapy. *Int J Mol Sci*. 2021;22(5):2251. doi:10.3390/ijms22052251
71. Urata C, Yamada H, Wakabayashi R, et al. Aqueous colloidal mesoporous nanoparticles with ethylene-bridged silsesquioxane frameworks. *J Am Chem Soc*. 2011;133(21):58102–58105. doi:10.1021/ja201779d
72. Zhou MY, Du X, Li WK, et al. One-pot synthesis of redox-triggered biodegradable hybrid nanocapsules with a disulfide-bridged silsesquioxane framework for promising drug delivery. *J Mater Chem B*. 2017;5(23):4455–4469. doi:10.1039/c6tb03368g
73. Sun Y, Chen M, Wu L. Controllable synthesis of hollow periodic mesoporous organosilica spheres with radial mesochannels and their degradable behavior. *J Mater Chem A*. 2018;6:12323–12333. doi:10.1039/C8TA02569J
74. Mai NXD, Nguyen TT, Vong LB, et al. Tailoring chemical compositions of biodegradable mesoporous organosilica nanoparticles for controlled slow release of chemotherapeutic drug. *Mat Sci Eng C Mater*. 2021;127:112232. doi:10.1016/j.msec.2021.112232
75. Fatiev Y, Croissant JG, Julfakyan K, et al. Enzymatically degradable hybrid organic-inorganic bridged silsesquioxane nanoparticles for in vitro imaging. *Nanoscale*. 2015;7(37):15046–15050. doi:10.1039/c5nr03065j
76. Liu CH, Cao Y, Cheng YR, et al. An open source and reduce expenditure ROS generation strategy for chemodynamic/photodynamic synergistic therapy. *Nat Commun*. 2020;11(1):1735. doi:10.1038/s41467-020-15591-4
77. Zheng NN, Wang Q, Li CL, et al. Responsive degradable theranostic agents enable controlled selenium delivery to enhance photothermal radiotherapy and reduce side effects. *Adv Healthc Mater*. 2021;10(10):2002024. doi:10.1002/adhm.202002024
78. Pohaku Mitchell KK, Liberman A, Kummel AC, et al. Iron (III)-doped, silica nanoshells: a biodegradable form of silica. *J Am Chem Soc*. 2012;134(34):13997–14003. doi:10.1021/ja3036114
79. Joseph MM, Ramya AN, Vijayan VM, et al. Targeted theranostic nano vehicle endorsed with self-destruction and immunostimulatory features to circumvent drug resistance and wipe-out tumor reinitiating cancer stem cells. *Small*. 2020;16(38):2003309. doi:10.1002/sml.202003309
80. Li X, Zhang LX, Dong XP, et al. Preparation of mesoporous calcium doped silica spheres with narrow size dispersion and their drug loading and degradation behavior. *Micropor Mesopor Mat*. 2007;102(102):151–158. doi:10.1016/j.micromeso.2006.12.048
81. Hao XH, Hu XX, Zhang CM, et al. Hybrid mesoporous silica-based drug carrier nanostructures with improved degradability by hydroxyapatite. *ACS Nano*. 2015;9(10):9614–9625. doi:10.1021/nn507485j
82. Chen MM, Hu JX, Bian CC, et al. pH-responsive and biodegradable ZnO-capped mesoporous silica composite nanoparticles for drug delivery. *Materials*. 2020;13(18):3950. doi:10.3390/ma13183950
83. Sun X, Zhang GL, Du RH, et al. A biodegradable MnSiO<sub>3</sub>@Fe<sub>3</sub>O<sub>4</sub> nanoplatform for dual-mode magnetic resonance imaging guided combinatorial cancer therapy. *Biomaterials*. 2019;194:151–160. doi:10.1016/j.biomaterials.2018.12.004
84. Liu CG, Han YH, Zhang JT, et al. Rerouting engineered metal-dependent shapes of mesoporous silica nanocontainers to biodegradable Janus-type (sphero-ellipsoid) nanoreactors for chemodynamic therapy. *Chem Eng J*. 2019;370:1188–1199. doi:10.1016/j.cej.2019.03.272
85. Zou R, Li JW, Yang T, et al. Biodegradable manganese engineered nanocapsules for tumor-sensitive near-infrared persistent luminescence/magnetic resonance imaging and simultaneous chemotherapy. *Theranostics*. 2021;11(17):8448–8463. doi:10.7150/thno.59840
86. Wang LY, Huo MF, Chen Y, et al. Iron-engineered mesoporous silica nanocatalyst with biodegradable and catalytic framework for tumor-specific therapy. *Biomaterials*. 2018;163:1–13. doi:10.1016/j.biomaterials.2018.02.018
87. Tang HX, Li CQ, Zhang Y, et al. Targeted manganese doped silica nano GSH-cleaner for treatment of liver cancer by destroying the intracellular redox homeostasis. *Theranostics*. 2020;10(21):9865–9887. doi:10.7150/thno.46771
88. Yang GB, Xu LG, Chao Y, et al. Hollow MnO<sub>2</sub> as a tumor microenvironment responsive biodegradable nano-platform for combination therapy favoring antitumor immune responses. *Nat Commun*. 2017;8(1):902. doi:10.1038/s41467-017-01050-0
89. Li XW, Zhao WR, Liu XH, et al. Mesoporous manganese silicate coated silica nanoparticles as multi-stimuli-responsive T1-MRI contrast agents and drug delivery carriers. *Acta Biomater*. 2016;30:378–387. doi:10.1016/j.actbio.2015.11.036
90. Wang XP, Li X, Ito A, et al. Biodegradable metal ions doped mesoporous silica nanospheres stimulate anti-cancer Th1 immune response in vivo. *ACS Appl Mater Inter*. 2017;9(50):43538–43544. doi:10.1021/acsmi.7b16118
91. Yang KK, Yue LD, Yu GC, et al. A hypoxia responsive nanoassembly for tumor specific oxygenation and enhanced sonodynamic therapy. *Biomaterials*. 2021;275:120822. doi:10.1016/j.biomaterials.2021.120822
92. Huang Y, Li P, Zhao R, et al. Silica nanoparticles: biomedical applications and toxicity. *Biomed Pharmacother*. 2022;151:113053. doi:10.1016/j.biopha.2022.113053
93. He QJ, Zhang ZW, Gao F, et al. In vivo biodistribution and urinary excretion of mesoporous silica nanoparticles: effects of particle size and PEGylation. *Small*. 2011;7(2):271–280. doi:10.1002/sml.201001459
94. Huang XL, Li LL, Liu TL, et al. The shape effect of mesoporous silica nanoparticles on biodistribution, clearance, and biocompatibility in vivo. *ACS Nano*. 2011;5(7):5390–5399. doi:10.1021/nn200365a
95. Fu CH, Liu TL, Li LL, et al. The absorption, distribution, excretion and toxicity of mesoporous silica nanoparticles in mice following different exposure routes. *Biomaterials*. 2013;34(10):2565–2575. doi:10.1016/j.biomaterials.2012.12.043

96. Lindén M. Biodistribution and excretion of intravenously injected mesoporous silica nanoparticles: implications for drug delivery efficiency and safety. *Enzymes*. 2018;43:155–180. doi:10.1016/bs.enz.2018.07.007
97. Liao YT, Liu CH, Yu J, et al. Liver cancer cells: targeting and prolonged-release drug carriers consisting of mesoporous silica nanoparticles and alginate microspheres. *Int J Nanomed*. 2014;9:2767–2778. doi:10.2147/IJN.S60171
98. Carvalho GC, Marena GD, Karnopp JCF, et al. Cetyltrimethylammonium bromide in the synthesis of mesoporous silica nanoparticles: general aspects and in vitro toxicity. *Adv Colloid Interface Sci*. 2022;307:102746. doi:10.1016/j.cis.2022.102746
99. Deng YD, Zhang XD, Yang XS, et al. Subacute toxicity of mesoporous silica nanoparticles to the intestinal tract and the underlying mechanism. *J Hazard Mater*. 2021;409:124502. doi:10.1016/j.jhazmat.2020.124502
100. Chauhan S, Manivasagam G, Kumar P, et al. Cellular toxicity of mesoporous silica nanoparticle in SHSY5Y and BMMNCs cell. *Pharm Nanotechnol*. 2018;6(4):245–252. doi:10.2174/2211738506666181031160108
101. Nasr SS, Nasra MMA, Hazzah HA, et al. Mesoporous silica nanoparticles, a safe option for silymarin delivery: preparation, characterization, and in vivo evaluation. *Drug Deliv Transl Res*. 2019;9(5):968–979. doi:10.1007/s13346-019-00640-3
102. Croissant JG, Butler KS, Zink JJ, et al. Synthetic amorphous silica nanoparticles: toxicity, biomedical and environmental implications. *Nat Rev Mater*. 2020;5:886–909. doi:10.1038/s41578-020-0230-0
103. Feng W, Zhou X, He C, et al. Polyelectrolyte multilayer functionalized mesoporous silica nanoparticles for pH-responsive drug delivery: layer thickness-dependent release profiles and biocompatibility. *J Mater Chem B*. 2013;1(43):5886–5898. doi:10.1039/c3tb21193b
104. Yamashita F, Hashida M. Pharmacokinetic considerations for targeted drug delivery. *Adv Drug Deliv Rev*. 2013;65(1):139–147. doi:10.1016/j.addr.2012.11.006
105. Wang B, He X, Zhang ZY, et al. Metabolism of nanomaterials in vivo: blood circulation and organ clearance. *Acc Chem Res*. 2013;46(3):761–769. doi:10.1021/ar2003336
106. Malfatti MA, Palko HA, Kuhn EA, et al. Determining the pharmacokinetics and long-term biodistribution of SiO<sub>2</sub> nanoparticles in vivo using accelerator mass spectrometry. *Nano Lett*. 2012;12(11):5532–5538. doi:10.1021/nl302412f
107. Yu Y, Wang Z, Wang R, et al. Short-term oral administration of mesoporous silica nanoparticles potentially induced colon inflammation in rats through alteration of gut microbiota. *Int J Nanomed*. 2021;16:881–893. doi:10.2147/IJN.S295575
108. Yu MX, Zheng J. Clearance pathways and tumor targeting of imaging nanoparticles. *ACS Nano*. 2015;9(7):6655–6674. doi:10.1021/acsnano.5b01320
109. Goel S, Ferreira CA, Dogra P, et al. Size-optimized ultrasoft porous silica nanoparticles depict vasculature-based differential targeting in triple negative breast cancer. *Small*. 2019;15(46):1903747. doi:10.1002/sml.201903747
110. Chen X, Zhouhua W, Jie Z, et al. Renal interstitial fibrosis induced by high-dose mesoporous silica nanoparticles via the NF-κB signaling pathway. *Int J Nanomed*. 2014;10:1–22. doi:10.2147/IJN.S73538
111. Dogra P, Adolph NL, Wang ZH, et al. Establishing the effects of mesoporous silica nanoparticle properties on in vivo disposition using imaging-based pharmacokinetics. *Nat Commun*. 2018;9(1):4551. doi:10.1038/s41467-018-06730-z
112. He YJ, Fan XY, Wu XZ, et al. pH-Responsive size-shrinkable mesoporous silica-based nanocarriers for improving tumor penetration and therapeutic efficacy. *Nanoscale*. 2022;14(4):1271–1284. doi:10.1039/d1nr07513f
113. Peng C, Huang Y, Zheng J. Renal clearable nanocarriers: overcoming the physiological barriers for precise drug delivery and clearance. *J Control Release*. 2020;322:64–80. doi:10.1016/j.jconrel.2020.03.020
114. Zhang XY, Luan JY, Chen W, et al. Mesoporous silica nanoparticles induced hepatotoxicity via NLRP3 inflammasome activation and caspase-1-dependent pyroptosis. *Nanoscale*. 2018;10(19):9141–9152. doi:10.1039/c8nr00554k
115. Tsoi KM, MacParland SA, Ma XZ, et al. Mechanism of hard-nanomaterial clearance by the liver. *Nat Mater*. 2016;15(11):1212–1221. doi:10.1038/nmat4718
116. Zhang YN, Poon W, Tavares AJ, et al. Nanoparticle-liver interactions: cellular uptake and hepatobiliary elimination. *J Control Release*. 2016;240:332–348. doi:10.1016/j.jconrel.2016.01.020
117. Lu JN, Liu FY, Li HJ, et al. Width-consistent mesoporous silica nanorods with a precisely controlled aspect ratio for lysosome dysfunctional synergistic chemotherapy/photothermal therapy/starvation therapy/oxidative therapy. *ACS Appl Mater Interfaces*. 2020;12(22):24611–24622. doi:10.1021/acsami.0c06117
118. Paula AJ, Araujo Júnior RT, Martinez DST, et al. Influence of protein Corona on the transport of molecules into cells by mesoporous silica nanoparticles. *ACS Appl Mater Interfaces*. 2013;5(17):8387–8393. doi:10.1021/am4014693
119. Wang Y, Gou K, Guo X, et al. Advances in regulating physicochemical properties of mesoporous silica nanocarriers to overcome biological barriers. *Acta Biomater*. 2021;123:72–92. doi:10.1016/j.actbio.2021.01.005
120. Hao N, Li L, Zhang Q, et al. The shape effect of PEGylated mesoporous silica nanoparticles on cellular uptake pathway in Hela cells. *Micropor Mesopor Mat*. 2012;162:14–23. doi:10.1016/j.micromeso.2012.05.040
121. Manzano M, Vallet-Regí M. Mesoporous silica nanoparticles for drug delivery. *Adv Funct Mater*. 2020;3(2):1902634. doi:10.1002/adfm.201902634
122. Souris JS, Lee CH, Cheng SH, et al. Surface charge-mediated rapid hepatobiliary excretion of mesoporous silica nanoparticles. *Biomaterials*. 2010;31(21):5564–5574. doi:10.1016/j.biomaterials.2010.03.048
123. Wu F, Chen PM, Gardinier TC, et al. Ultrasoft folate receptor alpha targeted enzymatically cleavable silica nanoparticle drug conjugates augment penetration and therapeutic efficacy in models of cancer. *ACS Nano*. 2022;16(12):20021–20033. doi:10.1021/acsnano.2c05342
124. Lee D, Beack S, Yoo J, et al. In vivo photoacoustic imaging of livers using biodegradable hyaluronic acid-conjugated silica nanoparticles. *Adv Funct Mater*. 2018;28:1800941. doi:10.1002/adfm.201800941
125. Zhou H, Li Q, Cheng X, et al. A Janus upconverting nanoplatform with biodegradability for glutathione depletion, near-infrared light induced photodynamic therapy and accelerated excretion. *J Mater Chem B*. 2020;8(40):9251–9257. doi:10.1039/d0tb01357a

## International Journal of Nanomedicine

Dovepress

**Publish your work in this journal**

The International Journal of Nanomedicine is an international, peer-reviewed journal focusing on the application of nanotechnology in diagnostics, therapeutics, and drug delivery systems throughout the biomedical field. This journal is indexed on PubMed Central, MedLine, CAS, SciSearch®, Current Contents®/Clinical Medicine, Journal Citation Reports/Science Edition, EMBase, Scopus and the Elsevier Bibliographic databases. The manuscript management system is completely online and includes a very quick and fair peer-review system, which is all easy to use. Visit <http://www.dovepress.com/testimonials.php> to read real quotes from published authors.

Submit your manuscript here: <https://www.dovepress.com/international-journal-of-nanomedicine-journal>